

AperTO - Archivio Istituzionale Open Access dell'Università di Torino

**Pre-Alpine Extensional Tectonics of a Peridotite-Localized Oceanic Core Complex in the Late Jurassic, High-Pressure Monviso ophiolite (Western Alps)**

**This is the author's manuscript**

*Original Citation:*

*Availability:*

This version is available <http://hdl.handle.net/2318/1540479> since 2018-06-14T10:07:56Z

*Published version:*

DOI:10.18814/epiiugs/2015/v38i4/82421

*Terms of use:*

Open Access

Anyone can freely access the full text of works made available as "Open Access". Works made available under a Creative Commons license can be used according to the terms and conditions of said license. Use of all other works requires consent of the right holder (author or publisher) if not exempted from copyright protection by the applicable law.

(Article begins on next page)



# UNIVERSITA' DEGLI STUDI DI TORINO

**This is an author version of the contribution published on:**

Questa è la versione dell'autore dell'opera:

*Balestro et al. (2015) -Episodes, v.38 (4), 266-282*

doi: 10.18814/epiiugs/2015/v38i4/82421

The definitive version is available at:

La versione definitiva è disponibile alla URL:

<http://www.episodes.org/>

17  
18 **Pre-Alpine Extensional Tectonics of a Peridotite-Localized Oceanic Core Complex in**  
19 **the Late Jurassic, High-Pressure Monviso ophiolite (Western Alps)**  
20

21 **<sup>1</sup>Gianni Balestro, <sup>1\*</sup>Andrea Festa, <sup>2</sup>Yildirim Dilek, and <sup>3</sup>Paola Tartarotti**

22  
23  
24 1: Dipartimento di Scienze della Terra, Università di Torino, Via Valperga Caluso, 35, 10125 - Torino, Italy

25 2: Department of Geology and Environmental Earth Science, Miami University, Oxford, OH 45056, USA

26 3: Dipartimento di Scienze della Terra, Università di Milano, Via Mangiagalli, 34, 20133 - Milano, Italy  
27  
28  
29  
30  
31  
32  
33  
34  
35  
36  
37  
38  
39  
40  
41  
42

43 **\*Corresponding author:**

44 Andrea Festa

45 E-mail: [andrea.festa@unito.it](mailto:andrea.festa@unito.it)

46 Phone: +39-0116705186  
47  
48  
49  
50  
51  
52  
53  
54  
55

56 EPISODES (Ophiolite Special Issue)  
57

58 **Abstract**

59

60 *The Late Jurassic Monviso ophiolite in the Western Alps is a multiply deformed, eclogite-facies meta-*  
61 *ophiolite that represents a remnant of the Alpine Tethyan oceanic lithosphere. The recent recognition*  
62 *of a pre-Alpine detachment fault in the Lower Tectonic Unit of this ophiolite has led to the discovery of*  
63 *an oceanic core complex, which developed during the initial stages of the tectonic evolution of the*  
64 *Alpine Tethys. The NNW-striking, 20–25-km-long shear zone (Baracun Shear Zone) contains ductilely*  
65 *to cataclastically deformed blocks and clasts of Fe-Ti and Mg-Al metagabbros in a matrix made of*  
66 *mylonitic serpentinite and talc-chlorite schist with high Ni–Cr concentrations and high Cl contents.*  
67 *Intensely sheared ophicarbonates and brecciated serpentinite within this shear zone are*  
68 *deformed by the Alpine-phase S1 foliation and D2 folds, providing a critical age constraint for the*  
69 *timing of its formation. Metabasaltic–metasedimentary rocks in the hanging wall increase in thickness*  
70 *away from the shear zone, characteristic of syn-extensional rock sequences in supradetachment*  
71 *basins. A Lower Cretaceous post-extensional sedimentary sequence unconformably cover the syn-*  
72 *extensional strata, the detachment shear zone, and the ophiolitic footwall, establishing a strong*  
73 *structural evidence for the intraoceanic, seafloor spreading origin of the tectonic fabric of the Monviso*  
74 *ophiolite, prior to the onset of subduction zone tectonics in the Alpine Tethys. The Monviso ophiolite*  
75 *and the Baracun Shear Zone represent a peridotite-localized oceanic core complex, which survived*  
76 *both the subduction and continental collision tectonic stages of the Alpine orogeny. Intraoceanic*  
77 *detachment faults and oceanic core complexes may play a significant role in subduction initiation, and*  
78 *hence their recognition in orogenic belts is an important step in reconstructing the record of ocean*  
79 *basin collapse and closure.*

80

81

## 82 1. Introduction

83

84

85

86

87

88

89

90

91

92

93

94

95

96

97

98

99

100

101

102

103

104

105

106

107

108

109

110

111

## 112 2. Regional Geology of the Western Alps and its Tethyan connection

113

114

115

116

117

118

119

120

121

122

123

124

125

126

127

128

129

130

131

132

Discontinuous exposures of the Late Jurassic, eclogitic ophiolite massifs in the Western Alps (Fig. 1) have been widely used in various studies to constrain the paleogeography of the Alpine Tethys, evolved between Europe and Adria during the Mesozoic. They, in particular, have been well utilized to determine the P-T-t trajectories of the Jurassic oceanic crust in a subduction-accretion system during the convergent–collision tectonic evolution of this orogenic belt (e.g., Frey et al., 1999). However, detailed, field-based structural, petrological and geochemical studies of the seafloor spreading and extensional tectonic history of these ophiolites have been scarce. This has been in part due to the strong overprint of the Alpine-stage subduction-collision related deformation–metamorphic events that obscures the previously developed rift-drift and seafloor spreading generated structures and mineral assemblages in these units.

In this paper, we document through detailed geological mapping, systematic structural and stratigraphic observations, petrographic and geochemical analyses the internal structure, tectonic fabric and evolution history of the Monviso ophiolite, one of the best preserved ophiolites in the Western Alps. We show that this ophiolite is an on-land exposure of an oceanic core complex, which formed through simple-shear seafloor spreading kinematics during the opening of the Ligurian–Piedmont ocean basin within the Alpine Tethys. This inferred oceanic core complex origin of the Monviso ophiolite is significant in that: (1) it better explains the dismembered and highly attenuated crustal architecture of the ophiolites in the Western Alps; (2) it presents a first coherent documentation of the intraoceanic extensional tectonic history of the Jurassic oceanic lithosphere preserved in the Western Alps, demonstrating that it is possible “to see through” the subduction–collision induced metamorphic overprint in multiply deformed orogenic belts; and (3) it provides a regionally consistent tectonic framework for the rift-drift, seafloor spreading, and contractional episodes of the Ligurian – Piedmont ocean basin evolution. Our data and observations from the Monviso ophiolite complement the diverse datasets available from the modern oceanic core complexes, and provide further insights into the geometry, internal structure, and stratigraphy of supradetachment basin sequences, which are missing from in-situ oceanic core complexes.

The Western Alps (Fig. 1) developed due to the collision between Adria (upper plate) and Europe (lower plate) as the intervening oceanic lithosphere of the Jurassic Alpine Tethys Ocean was consumed (see e.g. Coward and Dietrich 1989; Laubscher 1991; Dilek, 2006). The collision zone (i.e. the axial section of the Alpine belt) involves an exhumed fossil subduction complex bounded by the Penninic front and the Insubric and Canavese lines (Fig. 1A). Tectonic units of this subduction complex are overthrust WNW onto the European foreland (Ricou and Siddans, 1986; Platt et al. 1989; Schmid and Kissling 2000; Butler et al. 2013). Different meta-ophiolite units (i.e. the Piedmont Zone; see e.g. Dal Piaz et al., 2003) are tectonically sandwiched between the European and Adriatic continental margin units (see Bigi et al., 1990), and display varying metamorphic facies conditions ranging from high-pressure (HP) to ultra high-pressure (UHP) (Frey et al., 1999 and reference therein). The Piedmont Zone is distinguished by eclogite-facies units (i.e. the Zermatt-Saas Zone *auct.*; Bearth, 1967) and blueschist-facies ones (i.e. the Combin Zone *auct.*, Fig. 1A).

The orogenic structural architecture of the Western Alps as seen in the field today (Fig. 1) was built up during three main phases of deformation-metamorphism events (Balestro et al., 2015): (1) E-dipping subduction zone tectonics and eclogite-facies metamorphism in the Paleocene to middle Eocene, during which contractional deformation (D1) structures, mainly S1 foliation, were developed; (2) Continental collision tectonics in the late Eocene–early Oligocene that caused W-vergent folding and thrusting (D2). Blueschist- to greenschist-facies metamorphic re-equilibration took place during this event, producing S2 foliation; (3) Crustal exhumation (D3) and deep crust/mantle indentation in

133 the middle Oligocene to Neogene. Updoming of the partially subducted European continental margin,  
 134 the UHP Dora Maira, and the tilting of the Monviso ophiolite to the west (Fig. 1B) occurred during this  
 135 late Alpine stage evolution of the Western Alps (see, e.g., Lardeaux et al., 2006).

136 The meta-ophiolites in the Western Alps are the remnants of the Alpine Tethyan oceanic  
 137 lithosphere, which developed as a result of its rift-drift and seafloor spreading evolution (Elter, 1971;  
 138 Dal Piaz et al., 1972; Lemoine and Tricart., 1986; Stampfli and Marthaler, 1990; Dilek and Furnes,  
 139 2011, 2014). The timing of drifting and spreading has been constrained by U/Pb dating of ophiolitic  
 140 gabbros between 165 and 150 Ma (Manatschal and Müntener, 2009 for a review), and by the ages of  
 141 the initial post-rift sedimentary sequences (i.e. radiolarian chert) that overlap with the igneous ages of  
 142 gabbros (see Bill et al, 2001, for a review). Paleo-spreading rates in the Alpine Tethys are inferred to  
 143 have been slow- to ultraslow (~2 mm/yr) (see Lagabrielle, 2009, for a review), forming a Red Sea-  
 144 type, embryonic ocean (Lombardo et al., 2002). This ultraslow-spreading origin interpretation is based,  
 145 in part, on the occurrence of basaltic lava units directly resting on serpentinized peridotites. These  
 146 spatial relationships between upper mantle peridotites and lavas with sedimentary intercalations and  
 147 cover are well documented from modern oceanic core complexes, rifted continental margins, and  
 148 some other Tethyan ophiolites (Dilek and Delaloye, 1992; Dilek and Eddy, 1992; Dilek et al., 1998;  
 149 Miranda and Dilek, 2010; Manatschal et al., 2011; Festa et al., 2015a). Simple-shear extensional  
 150 deformation in these tectonic settings is shown to have exhumed the lithospheric mantle rocks on the  
 151 seafloor during the rift-drift and seafloor spreading stages of ocean basin evolution (Dilek and Thy,  
 152 1998; Dilek and Newcomb, 2003, and the papers therein).

### 155 3. Monviso ophiolite

156  
 157 The Monviso ophiolite occurs in the southern part of the Western Alps (Fig. 1), and is  
 158 tectonically sandwiched between the Dora Maira Unit (Internal Crystalline Massif *Auct.*), which  
 159 represents part of the subducted-exhumed European continental margin (e.g., Dal Piaz et al., 2003)  
 160 and the Queyras Schistes Lustrés Complex (Lemoine, 1971; Lombardo et al., 1978; Lemoine and  
 161 Tricart, 1986). The carbonate-rich metasedimentary sequence of *schistes lustrés* hosts large bodies of  
 162 ophiolites, which comprise ophicarbonates and metaperidotites with gabbroic intrusions. This  
 163 metasedimentary sequence includes discontinuous exposures of Middle-Late-Jurassic metachert  
 164 horizons and laterally continuous Upper Jurassic marble layers covering the entire igneous basement  
 165 (e.g., Tricart and Lemoine, 1991; Tricart and Schwartz, 2006).

166 The Monviso ophiolite consists mainly of serpentinized metaperidotites hosting large bodies of  
 167 both Mg-Al and Fe-Ti metagabbros. These metagabbros have Middle–Late Jurassic crystallization  
 168 ages ( $163 \pm 2$  Ma; Rubatto and Hermann, 2003). The upper mantle rocks are composed of lherzolite  
 169 and minor harzburgite, and are overlain along tectonic contacts by tholeiitic pillow metalavas, and an  
 170 Upper Jurassic – Lower Cretaceous meta-sedimentary sequence (Balestro et al., 2013). The Monviso  
 171 ophiolite has been divided into two major tectonic units on the basis of their different Alpine-stage P-T  
 172 metamorphic peaks (Fig. 1C). The *Lower Tectonic Unit* (LTU) includes the metaperidotites,  
 173 metagabbros, metabasalts, and a shear zone made of mylonitic serpentinite and talc-chlorite schist.  
 174 Overlying this unit along a WSW-dipping tectonic contact is the *Upper Tectonic Unit* (UTU), which is  
 175 composed mainly of metabasaltic lavas and metagabbro intrusions. The LTU lithologies display peak  
 176 metamorphic P-T conditions of 2.5 GPa – 550°C (Groppo and Castelli, 2010; Angiboust et al., 2012;  
 177 Balestro et al., 2014). The UTU lithologies show, on the other hand, peak metamorphic P-T conditions  
 178 of 2.2 GPa – 480°C (Angiboust et al., 2012). Thus, the ophiolite exhibits a major tectonic discontinuity  
 179 separating two different metamorphic domains in it. Another major tectonic discontinuity occurs within  
 180 the *Lower Tectonic Unit* (LTU), in which a NNW-striking, >20-km-long shear zone (Baracun Shear  
 181 Zone, BSZ) separates the serpentinized metaperidotites and metagabbros in its footwall from  
 182 metabasalt and syn-extensional metasedimentary rocks in the hanging wall (Fig. 2). Both the footwall  
 183 and hanging wall units are unconformably overlain by the Lower Cretaceous, post-extensional  
 184 metasedimentary rocks (Festa et al., 2015a).

185  
186  
187  
188  
189  
190  
191  
192  
193  
194  
195  
196  
197  
198  
199  
200  
201  
202  
203  
204  
205  
206  
207  
208  
209  
210  
211  
212  
213  
214  
215  
216  
217  
218  
219  
220  
221  
222  
223  
224  
225  
226  
227  
228  
229  
230  
231  
232  
233  
234  
235  
236

#### 4. Structural architecture and stratigraphy of the LTU

Different lithologies and the BSZ in the LTU are pervasively folded during D2 deformation (see Balestro et al., 2014, 2015; Festa et al., 2015a for major details; Fig. 2), forming tight to isoclinal folds accompanied by a SW- to W-dipping axial planar foliation (i.e. the S2 foliation). These D2 folds deform the earlier formed S1 foliation and the primary surfaces (i.e. the S0 sedimentary bedding and magmatic foliation). Extensional normal faults, representing the D3 stage of deformation, are commonly localized along lithological contacts and the attenuated limbs of the D2 folds.

We describe below the structural architecture of the BSZ and the stratigraphy and structure of various tectonostratigraphic units in its footwall and hanging wall blocks. We also define and describe the post-extensional metasedimentary sequence that onlap all these tectonic entities in the LTU. These descriptions are based largely on our detailed structural work and observations in the Colle del Baracun, Colle Armoine, and Colle di Luca (Fig. 2) sections of the Monviso ophiolite.

##### 4.1 Baracun Shear Zone (BSZ)

The BSZ is tens of meters thick and includes talc-chlorite schist and mylonitic serpentinite, containing blocks of metagabbro displaying a scale-independent block-in-matrix fabric (Figs. 3A-L); *sensu* Festa, 2011; Festa et al., 2012). Due to the macroscopic-scale folding (D2), the BSZ occurs at different structural levels within the ophiolite (Fig. 2). It does not contain any material derived from the lithological units in its hanging wall. It corresponds to the Lower Shear Zone of Angiboust et al. (2011) and to the Lago Superiore Shear Zone of Balestro et al. (2013).

In its type locality at Colle del Baracun, the BSZ includes a talc-chlorite schist matrix with distinct chlorite-, talc-, and amphibole-rich domains (Fig. 3C). The chlorite-rich domains consist of chlorite, magnetite, pistacite, and accessory apatite, magnetite, allanite and zircon, and mainly occur in rootless hinges of D2 folds, which folded the S1 foliation (Fig. 3M). Pre-D1 talc and chlorite lamellae are also included in apatite grains. Talc-rich domains in the talc-chlorite schist matrix are composed of talc and fine-grained magnetite, and occur in two different modes. In the first one, fine-grained aggregates of talc and magnetite appear within the D2 fold hinges. In the second mode, coarse-grained talc lamellae are oriented in the S2 foliation plane. Talc-rich domains are commonly folded together with chlorite-rich domains or form anastomosing crenulation cleavages with microlithons of the rock that contain S1 and S2 foliations (Fig. 3M; see also Fig. 3N). Amphibole-rich domains include fine-grained, light-green amphibole and minor chlorite. Calcite locally occurs between these different mineral domains in the matrix. In the Colle Armoine and Colle di Luca sections, the matrix consists of dm- to m-thick layers of talc-chlorite schist, which is interbedded within mylonitic serpentinite (Figs. 3D and 3E). The serpentinite consists mainly of antigorite and magnetite, with minor brucite, talc and carbonate.

Blocks of Fe-Ti metagabbro and Mg-Al metagabbro, ranging in size from few dm to several meters, widely occur within the talc-chlorite schist and in the mylonitic serpentinite matrix throughout the shear zone (Figs. 3A and 3D). These gabbro blocks are also folded by D2 folds, and locally occur as rootless fold hinges of D2 folds (Fig. 3B). Fe-Ti metagabbro blocks display a fine-grained, banded texture defining the S1 foliation and consisting of a mineral assemblage of garnet-omphacite-rutile eclogite with minor chlorite, Na-amphibole, albite, talc and quartz. Omphacite porphyroblasts locally preserve relics of the magmatic pyroxene and retain fine-grained intergrowths of quartz and amphibole. The amphibole is represented by Mg-hastingsitic hornblende replacing primary igneous pyroxene, and is a result of the pre-Alpine alteration of gabbroic rocks. Mg-Al metagabbro blocks are coarse-grained and more pervasively deformed in comparison to the Fe-Ti metagabbros. The mineral assemblages in these Mg-Al metagabbros include: (a) Cr-omphacite accompanied by actinolite, tremolite and chlorite, and replacing magmatic pyroxene, (b) aggregates of clinozoisite and albite pseudomorphs after the original plagioclase, and (c) aggregates of rutile and titanite pseudomorph after ilmenomagnetite.



237 Differently from the metagabbros in the footwall (see below), the metagabbro blocks embedded  
 238 in the BSZ do not show metasomatic rims (i.e. rodingitic reactions) against the serpentinite wallrock  
 239 and the talc-chlorite schist matrix. But, they are enveloped by dm-thick layers of a clast-supported  
 240 metabreccia (Figs. 3F-I), in which clasts are made of the same gabbroic rocks as in the blocks. This  
 241 metabreccia envelope around the metagabbro blocks within the BSZ occurs throughout the entire  
 242 LTU, and is overprinted by S1 foliation and D2 folds (Figs. 3H and 3I). We observe these mesoscopic  
 243 structures and deformation fabrics at microscopic scales, as well; both micro-clasts and the matrix are  
 244 foliated along the S1 foliation planes (Fig. 3L). These observations indicate that brecciation,  
 245 fragmentation of blocks, and embedding of micro-clasts within a matrix must have occurred before the  
 246 Alpine-stage deformation and the associated metamorphic overprint (see, Balestro et al., 2015, for  
 247 details).

#### 248 **4.2 BSZ footwall units**

249  
 250 The footwall block of the BSZ consists of serpentinitized metaperidotites and metagabbros  
 251 (Figs. 2 and 4). The serpentinitized metaperidotites derive from lherzolite and minor harzburgite (Fig.  
 252 5A), and consist of oriented aggregates of antigorite and magnetite (S2 foliation) with minor diopside,  
 253 Mg-chlorite, tremolite and Ti-clinohumite. The original mineral assemblage is partly preserved in low-  
 254 strain domains (e.g. in the cores of D2 folds exposed to the east of Colle Armoine), as evidenced by  
 255 the relics of clinopyroxene and orthopyroxene porphyroclasts, and by olivine and spinel grains which  
 256 are partially to entirely replaced by aggregates of antigorite and magnetite.

257 Metagabbro intrusions in the serpentinitized metaperidotites form meters to hectometers thick  
 258 and decameters to sub-kilometer long bodies. They range in texture from poorly foliated, coarse-  
 259 grained pegmatitic gabbros (e.g. South of Colle Armoine; Fig. 5B) to pervasively foliated, anisotropic  
 260 gabbros (Fig. 5C) (e.g. East of Colle del Baracun and West of Colle di Luca). Compositionally, they  
 261 represent two sub-groups: Mg-Al and Fe-Ti metagabbros. The Mg-Al metagabbros are characterized  
 262 by the occurrence of Cr-omphacite that replaced magmatic pyroxenes. The Fe-Ti metagabbros have a  
 263 well-preserved garnet-omphacite-rutile eclogitic assemblage, which defines the S1 foliation. Contacts  
 264 between the serpentinitized metaperidotites and metagabbros are generally marked by rodingitic  
 265 reaction rinds.

266 Serpentinite laced with irregular calcite vein networks (i.e., meta-ophicarbonates) is exposed  
 267 along the contact between the footwall unit and the BSZ (Figs. 5D and 5E). Both in the Colle del  
 268 Baracun and Colle Armoine sections, meta-ophicarbonates are few meters thick and shows a  
 269 progressive transition from massive serpentinite to brecciated serpentinite with a white carbonate  
 270 matrix, and up to a highly sheared meta-ophicarbonates rock (Fig. 5F). In the Colle di Luca section, the  
 271 meta-ophicarbonates occurrence is no more than 30 m in thickness. Calcite veins in the meta-  
 272 ophicarbonates rock are overprinted by S1 foliation and deformed by D2 folds, constraining the timing  
 273 of hydrothermal activity that was responsible for the formation of ophicarbonates to a pre-Alpine stage  
 274 (Festa et al., 2015a).

#### 275 **4.3 BSZ hanging wall unit**

276  
 277 The hanging wall block of the BSZ includes metasedimentary and metabasaltic rocks spatially  
 278 associated with minor metagabbro occurrences (Figs. 2 and 4). Metasedimentary units consist of  
 279 calcschist layers interbedded with decimeters to sub-decameter thick horizons of mafic  
 280 metasandstone and metabreccia (Figs. 2 and 4). The type locality of these rocks is at Colle del  
 281 Baracun (Figs. 6A-C), where calcschist layers overlap the BSZ. The thickness of the entire calcschist  
 282 unit increases from zero to 70 meters away from the shear zone (Figs. 2 and 4; see also Balestro et  
 283 al., 2015; Festa et al., 2015a for details). At a regional scale and across the whole ophiolite, the  
 284 thickness of the metasedimentary unit gradually decreases toward the south (i.e. between Colle  
 285 Armoine and Colle di Luca sections). To the SW of Colle di Luca, a tens of meters – thick mafic  
 286 metabreccia represents the syn-extensional unit.



289 The calcschist consists of subparallel layers of carbonate minerals (i.e. calcite, minor dolomite  
 290 and ankerite), quartz and white mica, with subordinate chloritoid, Mg-Fe chlorite, zoisite, and textural  
 291 relics of lawsonite with graphite flakes. A matrix-supported mafic metabreccia unit is interbedded with  
 292 calcschist layers, and shows a fining-upward texture with sub-angular to angular clasts of gabbroic  
 293 rocks (Fig. 6B). The metabreccia is laterally gradational into tens of meters – thick metasandstone,  
 294 containing similar composition but much smaller size clasts (Figs. 4 and 6C). The matrix of the mafic  
 295 metabreccia and metasandstone is made of angular to irregularly shaped micro-clasts and grains,  
 296 composed of omphacite and aggregates of chlorite, Cr-rich white mica, and epidote (pistacite). All  
 297 these grains are in turn embedded in a groundmass of zoisite, light-green amphibole, epidote, albite,  
 298 chlorite, sphene, quartz and white mica. These textural relationships at various scales indicate the  
 299 detrital sedimentary nature of the protoliths of the mafic metabreccia and metasandstone.

300 The metabasaltic unit in the hanging wall of the BSZ is well exposed in the Colle Armoine  
 301 section. It gradually decreases in thickness from this locale both toward Colle del Baracun and Colle di  
 302 Luca (Figs. 2 and 4), and tapers out near Colle di Luca in the south. Mg-Al metagabbro outcrops with  
 303 fine-grained metabasaltic dikes are in contact with metabasalts north of Colle di Luca. The primary  
 304 breccia texture is still visible and well preserved in the metabasalt despite the strong overprint of a well  
 305 developed S2 foliation, defined by alternating layers of light green-yellow albite, epidote, clinozoisite  
 306 with minor white mica, and dark-green layers of Na-Ca amphibole, garnet and chlorite.

307

#### 308 **4.4 Post-extensional metasedimentary sequence**

309

310 The footwall and hanging wall lithological units (syn-extensional metasedimentary and  
 311 metabasaltic rocks) of the BSZ are unconformably overlain by a calcschist unit, which contains dm-  
 312 thick marble beds (Figs. 2, 4, 7A and 7B), passing upward into layered-foliated quartz-schist devoid of  
 313 any ophiolite-derived detrital material. On the basis of a regional correlation of this calcschist-marble-  
 314 quartz schist unit with other metasedimentary rocks in the Western Alps, Lagabrielle (1994)  
 315 established the age of the calcschist and the overlying syn-extensional rocks as the Lower  
 316 Cretaceous. Festa et al. (2015a) defined these metasedimentary rocks in the hanging wall of the BSZ  
 317 as post- extensional depositional units. The thickness of the post-extensional metasedimentary  
 318 sequence within the Monviso ophiolite is irregular (Fig. 2) and ranges from few meters to tens of  
 319 meters.

320 The calcschist unit consists of calcite, and minor dolomite with ankerite, quartz and white mica,  
 321 whereas the marble and quartz-rich schist are made of calcite and quartz, respectively. The contact  
 322 between the post-extensional metasedimentary units and both the syn-extensional sedimentary  
 323 sequence and the talc-chlorite schist of the BSZ is sharp and rugged (Figs. 7C-F), and corresponds to  
 324 an original depositional surface as inferred from the lack of any mylonitic structure associated with it  
 325 (Figs. 7E and 7F). This unconformity is folded together with the BSZ and the hanging wall and footwall  
 326 units as seen at different structural levels in the field (Fig. 2).

327

### 328 **5. Geochemistry and mineralogy of the BSZ**

329

330 The composition of the talc-chlorite schist rocks within the BSZ was determined by major- and  
 331 trace element chemistry analyses of selected rock samples, and by electron microprobe mineral  
 332 analyses. The bulk rock geochemistry of the talc-chlorite schist was then compared with the  
 333 compositional fields of the spatially associated serpentinite and metagabbro (Fig.8). Compared to the  
 334 serpentinite, the talc-chlorite schist rocks have higher values of SiO<sub>2</sub>, Al<sub>2</sub>O<sub>3</sub> and CaO, show lower  
 335 values of MgO, and are characterized by particularly strong enrichment in TiO<sub>2</sub>. On the other hand,  
 336 compared to the metagabbro, the talc-chlorite schist is depleted in Al<sub>2</sub>O<sub>3</sub>, CaO, total Fe and Na<sub>2</sub>O,  
 337 enriched in MgO. The talc-rich rock also shows high absolute concentrations of Cr, Ni and V.

338 Electron microprobe mineral chemistry analyses reveal that chlorite in the talc-chlorite schist  
 339 predominantly has a penninite (i.e., a Mg-rich solid solution between serpentine and amesite)  
 340 composition (XMg=[0,83-0,89]), with minor pycnochlorite (XMg= 0,79) and clinochlore (XMg= 0,84-

341 0,85) components. Some zoned chlorite grains are significantly enriched in Cr and in Ni in their  
 342 centers. Chlorite also has relatively high chlorine content (up to 500 ppm).

343 Electron microprobe mineral chemistry analyses have shown that talc in the talc-chlorite schist  
 344 is characterized by a negligible substitution of Mg by Fe ( $X_{Fe}=[0,04-0,09]$ ), and that it contains high  
 345 NiO concentrations (highest NiO= 0,32 wt% in talc lamellae included in apatite). Talc also has  
 346 relatively high chlorine contents (up to 900 ppm).

347

348

## 349 **6. Discussion**

350

351 In this section, we discuss in a regional tectonic framework the significance of our structural,  
 352 mineralogical and geochemical data, field observations, and interpretations from the Monviso ophiolite  
 353 for: (1) its oceanic core complex origin, (2) the timing of this extensional tectonic episode and core  
 354 complex development, and (3) the maturation of the Ligurian–Piedmont basin as a supradetachment  
 355 depocenter within the Alpine Tethys.

356

### 357 **6.1 Oceanic core complex origin of the Monviso ophiolite and the BSZ**

358

359 The structural, textural and mineralogical evidence collectively indicate that the BSZ played a  
 360 significant role in accommodating high-magnitude extension in young oceanic lithosphere and in the  
 361 exhumation of lower crustal gabbros and upper mantle peridotites to the seafloor within the Ligurian-  
 362 Piedmont ocean basin. This simple-shear extensional tectonics produced a Late Jurassic oceanic core  
 363 complex, which is now represented by the multiply deformed Monviso ophiolite in the Western Alps  
 364 (Figs. 9 and 10B). We infer that the mafic metabreccia within the BSZ and the talc-chlorite schist and  
 365 mylonitic serpentinite matrix surrounding the metagabbro blocks represent a Late Jurassic intra-  
 366 oceanic detachment fault. This low-angle detachment fault, which is now exposed along a 20-25-km-  
 367 long (Fig. 2), NNW-striking and W-to SW-dipping shear zone (Baracun Shear Zone), controlled the  
 368 seafloor spreading tectonics and the exhumation of upper mantle peridotites on the seafloor as an  
 369 oceanic core complex (Fig. 9). The kinematics of detachment faulting and the mode of the inferred  
 370 uplift and exhumation of the upper mantle rocks in the footwall of the BSZ (Figs. 9 and 10B) are  
 371 analogous to those documented from the in-situ core complexes along the slow- (Atlantis Massif, Mid-  
 372 Atlantic Ridge – MAR) and ultraslow-spreading (Atlantis Bank, Southwest Indian Ridge – SWIR)  
 373 ridges (Cannat, 1993; Tucholke et al., 1998; Boschi et al., 2006; Karson et al., 2006; Dick et al., 2008).

374 Based on the results of the drilling and submersible studies of the Atlantis Bank (SWIR) and  
 375 the Atlantis Massif (MAR), Miranda and Dilek (2010) defined gabbro-localized and peridotite-localized  
 376 oceanic core complexes, respectively. In a gabbro-localized core complex, high-temperature, crystal-  
 377 plastic deformation fabrics concentrate in the gabbros, and granulite-grade mylonitic rocks and shear  
 378 zones appear to have formed the nucleation of detachment-related deformation in the presence of  
 379 melt (Miranda and Dilek, 2010, and the references therein). In this type of oceanic core complex (such  
 380 as SWIR), the footwall of the detachment fault includes widespread gabbroic intrusions in the  
 381 serpentinitized peridotites. In a peridotite-localized core complex, gabbroic intrusions in the footwall  
 382 peridotites are less abundant in comparison to those in gabbro-localized core complexes, and the  
 383 crystal-plastic deformation fabrics occur both in peridotites and gabbros with increasingly more  
 384 abundant low-T°C fabric elements affecting the serpentinitized peridotites. Detachment faulting appears  
 385 to have nucleated mainly in the peridotites in which strain partitioning and formation of talc-  
 386 amphibolite-chlorite schists were taking place at temperatures more than 500°C, following the  
 387 emplacement of dispersed gabbros. The internal structure of the Monviso ophiolite and the BSZ  
 388 detachment fault is more akin to that of a peridotite-localized oceanic core complex, such as the  
 389 Atlantis Massif along the Mid-Atlantic Ridge (30° Latitude). We posit that emplacement of the Fe-Ti  
 390 and Mg-Al gabbros in the Monviso ophiolite and serpentinitization of the peridotites along syn-kinematic  
 391 fracture networks promoted rheological weakening of the ultramafic rocks and the development of the  
 392 low-angle BSZ (MacLeod et al., 2002).

393 The upper mantle peridotites and oceanic lower crustal units exposed on the seafloor along the  
 394 MAR commonly occur in the footwalls of detachment faults, which are characterized by tens to  
 395 hundreds of meters thick, ductile to cataclastic shear zones (Figs. 10A, 10C, and 10D; Boschi et al.,  
 396 2006, and reference therein). These structural fabrics represent the artifacts of hydrothermal fluid flow  
 397 and associated metasomatism, greenschist to sub-greenschist facies metamorphism (Escartin et al.,  
 398 2008), and strain partitioning in heterogeneously distributed rocks below the detachment surface. The  
 399 ubiquitous occurrence of talc-chlorite schist provides a weakening mechanism to allow a low-angle  
 400 normal fault to initiate and to localize strain over long periods of time (Escartin et al., 2008).

401 Our observations in the Monviso ophiolite indicate a progressive transition from massive  
 402 serpentinites to meta-ophicarbonates rocks, and higher up to a talc-chlorite schist shear zone, which  
 403 represents the Late Jurassic detachment fault (Figs. 10B, 10E and 10F). Low-angle faulting in this  
 404 case was accompanied by extensive hydrothermal metasomatism. Our microstructural observations  
 405 and mineral chemistry data suggest that the talc-chlorite schist along the BSZ was a result of rock–  
 406 fluid interactions between the gabbros and serpentinite, and seawater-derived hydrothermal fluids.  
 407 High Ni and Cr concentrations in this schist rock are compositionally similar to those of chlorite and  
 408 talc documented from detachment zone fault rocks in both the modern (Boschi et al., 2006) and  
 409 ancient (Manatschal et al., 2011) oceanic core complexes. The relatively high chlorine contents in the  
 410 talc-chlorite schist along the BSZ highlight the role of seawater-derived hydrothermal fluids percolating  
 411 along–across the shear zone. Talc-rich rocks may form at early stages of faulting by interaction of  
 412 hydrothermal fluids with upper mantle rocks exhumed to shallow depths on their way to the seafloor.  
 413 This metasomatic process is critical in rheological weakening and strain localization, and facilitates the  
 414 propagation of deformation farther down into the footwall rocks beneath the detachment surface,  
 415 resulting in thickening of the detachment-induced shear zone (Fig. 10). Further propagation of brittle  
 416 faults and fractures into the peridotites and gabbros in the footwall must have provided preferential  
 417 pathways for seawater penetration and attendant hydration and serpentinitization of the ultramafic  
 418 rocks. This serpentinitization process was likely to have contributed to the footwall uplift and  
 419 exhumation, as documented from the MARK (Mid-Atlantic Ridge at Kane Fracture Zone) area in the  
 420 modern oceanic lithosphere (Dilek et al., 1997).

## 422 **6.2. Timing of oceanic lithosphere formation in the Ligurian – Piedmont Ocean**

423  
 424 Diachronous crystallization ages of gabbros in the ophiolites of the Western Alps have been  
 425 widely used for reconstructing the tectonic history of the Ligurian – Piedmont ocean basin (e.g.,  
 426 Lombardo et al., 2002; Piccardo, 2009; Manatschal and Müntener, 2009). Assuming that the igneous  
 427 ages of the ophiolitic gabbros reflect the magmatic accretion of oceanic lithosphere, the seafloor  
 428 spreading and the extensional tectonic history of the Ligurian-Piedmont oceanic lithosphere can be  
 429 quantified temporally. The zircon U/Pb ages of the gabbro bodies within the Western Alps ophiolites  
 430 (Fig. 11) range from 166±1 Ma (in Gets) to 155±1.2 Ma (in Antrona) (see, e.g., Lombardo et al., 2002  
 431 and Manatschal and Müntener, 2009, and reference therein), showing a close overlap with the  
 432 biostratigraphic ages of the metaradiolarites spatially associated with the metabasalts. These ages  
 433 collectively suggest that the oceanic lithosphere in the northern part of the Ligurian – Piedmont Ocean  
 434 (Gets, 166±1 Ma) and in the Zermatt-Saas (Allain gabbro, 163±5 Ma) meta-ophiolites formed nearly  
 435 10 m.y. before than the oceanic lithosphere, now preserved in the Antrona section (155±2 Ma) to the  
 436 north. Farther to the south in the Western Alps, the igneous ages of the gabbros (163±2 My, Rubatto  
 437 and Hermann, 2003; and Lanzo massif, 162±2 Ma; Kaczmarek et al., 2008) are nearly coeval with  
 438 those of the Voltri and Corsica ophiolite units (see, e.g., Piccardo, 2009; Fig. 11). Younger zircon U/Pb  
 439 ages obtained from plagiogranites (Fig. 11) in the Monviso ophiolite (152±2 Ma, Lombardo et al.,  
 440 2002) and in the Chenalliet ophiolite massif (153±3 Ma, Costa and Caby, 2001) likely represent a late-  
 441 stage, off-axis magmatic episode in the igneous accretion history of the Ligurian – Piedmont oceanic  
 442 lithosphere (see Lombardo et al., 2002). This latest pulse of magmatism in the Monviso ophiolite  
 443 predated the unconformable deposition of the Lower Cretaceous post-extensional sediments overlying  
 444 the intraoceanic Baracun detachment fault zone (BSZ).

445 The unconformity surface at the base of the Lower Cretaceous post-extensional sedimentary  
 446 sequence seals the BSZ and onlaps both its hanging wall and footwall blocks. These stratigraphic  
 447 relationships indicate that the structural architecture documented from the LTU of the Monviso  
 448 ophiolite and the BSZ predates the deposition of these post-extensional rocks. Thus, the structural  
 449 fabric elements and the primary mineral assemblages recorded in the rock units of the ophiolite and  
 450 the BSZ reflect the rift-drift and seafloor spreading tectonic processes that took place during the  
 451 opening of the Ligurian – Piedmont ocean basin prior to the Early Cretaceous.

452 The exhumation of the upper mantle peridotites in the footwall and the deposition of the syn-  
 453 extensional sediments in the hanging wall of the BSZ occurred during the Late Jurassic. We can  
 454 constrain the specific timing of this extensional phase as between post  $163\pm 2$  Ma (Middle Callovian),  
 455 which is the crystallization age of the gabbroic intrusions in the peridotites (Rubatto and Hermann,  
 456 2003) and the Early Cretaceous, which is the depositional age of the post-extensional sedimentary  
 457 sequence above the unconformity. Meta-radiolarite rocks in the Queyras Schistes Lustrés Complex  
 458 (Caby et al., 1987) represent the stratigraphic base of the post-extensional sequence and reveal a  
 459 middle-late Oxfordian age for their deposition that is consistent with the age bracket we consider for  
 460 the timing of simple-shear extension and detachment faulting.

461 The lack of any material or blocks within the BSZ derived from the hanging wall  
 462 metasedimentary units or metabasaltic rocks also indicates that the main phase of detachment faulting  
 463 must have occurred before the Alpine stage deformation. Although subduction- to exhumation-related  
 464 tectonic reworking of the Ligurian – Piedmont oceanic lithosphere and the associated metamorphic  
 465 overprints partly obliterated the seafloor spreading history of the BSZ, its pre-Alpine stage record can  
 466 be well constrained by several lines of meso- to micro-scale structural evidence: (1) ophicarbonates  
 467 resting on the massive serpentinite indicate that the upper mantle peridotites were already  
 468 exhumed on the seafloor prior to the onset of subduction zone tectonics within the ocean basin. (2)  
 469 pre-D1 metabreccia enveloping the metagabbro blocks within the BSZ represents a fault rock that  
 470 formed during detachment faulting and the associated cataclastic deformation. (3) talc-chlorite schist  
 471 matrix in the BSZ represents a metamorphic assemblage, which typically develops along intraoceanic  
 472 detachment fault zones (see e.g., Boschi et al., 2006, and reference therein) due to syn-kinematic  
 473 alteration at the contact between serpentinitized peridotites and gabbros.

### 475 **6.3 Mature Ligurian–Piedmont ocean basin as a supradetachment depocenter**

477 The lateral and vertical facies variations in the meta-sedimentary sequences of the Monviso  
 478 ophiolite and the structural relationships of these sequences with the mantle peridotites provide  
 479 important clues for the nature of their depocenter within the Ligurian-Piedmont ocean basin.  
 480 Development of this depocenter and its accommodation space was strongly controlled by asymmetric  
 481 extension and tectonically controlled subsidence in the hanging wall of the low-angle Baracun  
 482 detachment shear zone (Fig. 9). The Upper Jurassic syn-extensional sedimentary succession with  
 483 abundant ophiolitic material onlaps the shear zone and its talc-chlorite schist rocks, and has a wedge  
 484 shape geometry with its thickest section corresponding to the distal depocenter of the  
 485 supradetachment basin.

486 The irregular thickness of the post-extensional sequence and its unconformable deposition on  
 487 top of the footwall and hanging wall (metabasalts and metasediments) sequences and the BSZ rocks  
 488 suggests an irregular seafloor bathymetry within the basin that was likely controlled by basement  
 489 faulting and tectonic segmentation (Fig. 9). The thinner and incomplete sections of this sequence  
 490 occur in the eastern part of the ophiolite where the Lower Cretaceous carbonate-rich calcschists  
 491 directly overlie the BSZ (Fig. 9). We interpret these bathymetric anomalies and the associated  
 492 stratigraphic variations as tectonically controlled structural highs within a basin, which was deepening  
 493 to the west (in the present coordinate system).

494 The initial input of continentally derived sediments within this basin did not occur until the  
 495 deposition of the uppermost part of the post-extensional sequence that contains quartz-rich  
 496 intercalations within the carbonate-rich calcschists. We postulate that this stage of deposition



497 coincided with significant terrigenous input into the basin. In comparison with the analogous post-  
498 extensional sequences preserved in the unmetamorphosed Ligurian Units of the Northern Apennines  
499 (see, e.g., [Decandia and Elter, 1972](#); [Marroni et al., 2010](#); [Festa et al., 2013](#), and references therein),  
500 we interpret these post-extensional deposits to represent distal carbonatic and mixed siliciclastic-  
501 carbonatic turbidites (i.e., Calpionella Limestone and/or Palombini Shale) which reworked a  
502 continental margin source area.

503

504

## 505 **7. Conclusions**

506

507 This study is a first systematic documentation, from the Western Alps, of the seafloor  
508 spreading and oceanic core complex development history of the Late Jurassic Monviso ophiolite,  
509 which experienced subduction zone deformation and high-P metamorphism following its magmatic  
510 construction. Our structural, stratigraphic, mineralogical and geochemical analyses of the footwall and  
511 hanging wall tectonostratigraphic units in the ophiolite indicate that the upper mantle peridotites and  
512 their Fe-Ti and Mg-Al gabbroic intrusions were uplifted and exhumed on the seafloor as in an  
513 intraoceanic core complex. Emplacement of gabbroic intrusions into the ultramafic rocks, widespread  
514 extensional fracturing and attendant serpentinization in the peridotites, and hydrothermal  
515 metasomatism associated with faulting were instrumental in the localization of a low-angle detachment  
516 shear zone in the upper mantle. Peridotite rocks within this shear zone experienced crystal-plastic  
517 fabric development, recrystallization of talc-chlorite schist, and cataclastic brecciation, as shown from  
518 the modern peridotite-localized core complexes along the Mid-Atlantic Ridge seafloor spreading  
519 environment.

520 The timing of intraoceanic core complex development in the Piedmont-Ligurian ocean basin, as  
521 preserved in the Monviso ophiolite, is well constrained to have taken place between Middle Callovian  
522 ( $163\pm 2$  Ma) and the middle-late Oxfordian. These ages reflect the timing of the emplacement of the  
523 gabbroic intrusions in the peridotites, and of the deposition of the post-extensional sedimentary  
524 sequence unconformably overlying the detachment shear zone and the syn-extensional deposits.  
525 Ophicarbonates and mafic breccias at the bottom of the syn-extensional deposits in the hanging wall  
526 record the early history of tectonically-induced sedimentation and accommodation space development  
527 above the shear zone. The wedge-shape geometry of the syn-extensional sequence, which thickens  
528 away from the Baracun shear zone, suggests a distal depocenter geometry as in a supradetachment  
529 basin configuration. Carbonate-rich calcshist with quartz-rich layers unconformably overlying the syn-  
530 extensional sequence and the ophiolite represent the post-extensional phase of deposition. The  
531 existence of continentally derived detrital material in this post-extensional sequence points to the  
532 proximal position of a continental margin to the Ligurian–Piedmont basin at this time.

533 The occurrence of a seafloor spreading originated oceanic core complex in the Monviso  
534 ophiolite is globally significant for two reasons: (1) Despite the strong overprint of subduction zone  
535 deformation and metamorphism, the simple-shear, intraoceanic extensional tectonic fabric is well  
536 preserved in the Late Jurassic oceanic lithosphere. This case study clearly demonstrates that not all  
537 shear zones, brittle-ductile and cataclastic structures, and highly dismembered ophiolites in high-  
538 pressure collisional belts generally represent the products of a subduction channel and subduction  
539 zone tectonics, as has been widely assumed in the literature pertaining to the Western Alps (i.e.,  
540 [Guillot et al., 2009](#); [Angiboust et al., 2011](#)). (2) Oceanic core complexes and their lithospheric-scale  
541 asymmetric shear zones (detachment faults) may be ideal tectonic settings for the localization of  
542 subduction initiation, as has been proposed from some other Tethyan ophiolites (i.e., [Maffione et al.,](#)  
543 [2015](#)). We think that inversion of extensional detachment faults into intraoceanic subduction zones  
544 under favorable geodynamic conditions provides a viable mechanism for basin collapse and closure  
545 without invoking other external driving forces in a given region.

546

## 547 **Acknowledgments**

548

549 This research has been supported by the following grants: (1) “ex 60%–2013 and 2014” Università  
 550 degli Studi di Torino and PROGEO Piemonte (Università degli Studi di Torino and Compagnia San  
 551 Paolo) to A. Festa and G. Balestro, (2) the Italian Ministry of University and Research Cofin-PRIN  
 552 2010/2011 (“GEOPROB–GEOdynamic Processes of Oceanic Basins” to A. Festa and P. Tartarotti,  
 553 and (3) “Subduction and exhumation of continental lithosphere: Implications on orogenic architecture,  
 554 environment and climate” to G. Balestro. We gratefully acknowledge these funds. We thank M.  
 555 Marroni, J. Wakabayashi and several other colleagues for providing us with insightful feedback and  
 556 comments on various aspects of our study in the Monviso ophiolite, as presented in this paper.  
 557

## 558 559 **References** 560

- 561 Angiboust, S., Agard, P., Raimbournh, H., Yamato, P., and Huet, B., 2011, Subduction interface  
 562 processes recorded by eclogite-facies shear zones (Monviso, W. Alps): *Lithos*, v. 127, pp. 222–  
 563 238. doi:10.1016/j.lithos.2011.09.004
- 564 Angiboust, S., Langdon, R., Agard, P., Waters, D., and Chopin, C., 2012, Eclogitization of the Monviso  
 565 ophiolite (W. Alps) and implications on subduction dynamics: *Journal of Metamorphic Geology*, v.  
 566 30, pp. 37–61. doi:10.1111/j.1525-1314.2011.00951.x
- 567 Balestro, G., Fioraso, G., and Lombardo, B., 2011, Geological map of the upper Pellice Valley (Italian  
 568 Western Alps): *Journal of Maps*, 2011, pp. 634-654. doi: 10.4113/jom.2011.1213.
- 569 Balestro, G., Fioraso, G., and Lombardo, B., 2013, Geological map of the Monviso massif (Western  
 570 Alps): *Journal of Maps*, v. 9 (4), pp. 623-634. doi: 10.1080/17445647.2013.842507.
- 571 Balestro, G., Lombardo, B., Vaggelli, G., Borghi, A., Festa, A., and Gattiglio, M., 2014,  
 572 Tectonostratigraphy of the northern Monviso Meta-ophiolite Complex (Western Alps): *Italian  
 573 Journal of Geosciences*, v. 133 (3), pp. 409-426. Doi: 10.3301/IJG.2014.13
- 574 Balestro, G., Festa, A., and Tartarotti, P., 2015, Tectonic significance of different block-in-matrix  
 575 structures in exhumed convergent plate margins: examples from oceanic and continental HP rocks  
 576 in Inner Western Alps (northwest Italy): *International Geology Review*, v. 57, no. 5-8, 581-605.  
 577 <http://dx.doi.org/10.1080/00206814.2014.943307>.
- 578 Bearth, P., 1967, Die Ophiolithe der Zone von Zermatt-Saas Fee: *Beiträge zur Geologischen Karte der  
 579 Schweiz, Neue Folge*, 132, 130 pp.
- 580 Bigi, G., Castellarin, A., Coli, M., Dal Piaz, G.V., Sartori, R., Scandone, P. and Vai, G.B., 1990,  
 581 Structural Model of Italy, sheets 1-2: CNR, Progetto Fin. Geodinamica, SELCA Firenze
- 582 Bill, M., O'Dogherty, L., Guex, J., Baumgartner, P.O., Masson, H., 2001, Radiolarite ages in Alpine-  
 583 Mediterranean ophiolites: constraints on the oceanic spreading and the Tethys-Atlantic  
 584 connection: *Geological Society of America Bulletin*, v. 113, pp. 129–143.
- 585 Borsi, L., Schärer, U., Gaggero, L., and Crispini, L., 1996, Age, origin and geodynamic significance of  
 586 plagiogranites in Iherzolites and gabbros of the Piedmont-Ligurian ocean basin: *Earth and  
 587 Planetary Science Letters*, v. 140, pp. 227–241.
- 588 Boschi, C., Früh-Green, G.L., and Delacour, A., 2006, Mass transfer and fluid flow during detachment  
 589 faulting and development of an oceanic core complex, Atlantis Massif (MAR 30°N): *Geochemistry,  
 590 Gephysics, Geosystem*, v. 7, doi: 10.1029/2005GC001074.
- 591 Bousquet, R., Schimid, S.M., Zeilinger, G., Oberhansli, R., Roseberg, C., Molli, G., Robert, C.,  
 592 Wiederkehr, M., Rossi, Ph., 2012, Tectonic framework of the Alps: CCGM/CGMW. 1 sheet.
- 593 Butler, J.P., Beaumont, C., and Jamieson, R.A., 2013, The Alps 1: A working geodynamic model for  
 594 burial and exhumation of (ultra)high-pressure rocks in Alpine-type orogens: *Earth and Planetary  
 595 Science Letters*, v. 377–378, pp. 114–131. doi:10.1016/j.epsl.2013.06.039
- 596 Caby R., Dupuy C. and Dostal J., 1987, The very beginning of the Ligurian Tethys in the Western  
 597 Alps: Petrological and geochemical evidence from the oldest ultramafite-derived sediments in  
 598 Queyras, Western Alps (France): *Eclogae Geologicae Helvetiae*, v. 80, pp. 223-240.  
 599

- 600 Cannat, M., 1993, Emplacement of mantle rocks in the seafloor at Mid-Ocean ridge: *Journal of*  
601 *Geophysical Research*, v. 98, B3, pp. 4163-4172.
- 602 Costa, S., and Caby, R., 2001, Evolution of the Ligurian Tethys in the Western Alps: Sm/Nd and U/Pb  
603 geochronology and rare-earth element geochemistry of the Montgenèvre ophiolite (France):  
604 *Chemical Geology*, v. 175, pp. 449–466.
- 605 Coward, M.P., and Dietrich, D., 1989, Alpine tectonics—an overview, in Coward M.P., Dietrich D.,  
606 Park R.G., eds., *Alpine tectonics: Geological Society of London Special Publications*, v. 45, pp. 1–  
607 29. doi:10.1144/GSL.SP.1989.045.01.01
- 608 Dal Piaz, G.V., Bistacchi, A., and Massironi, M., 2003, Geological outline of the Alps: *Episodes*, v. 26,  
609 pp. 175–180.
- 610 Dal Piaz, G.V., Hunziker, J.C., and Martinotti, G., 1972, La zona Sesia–Lanzo e l'evoluzione tettonico  
611 metamorfica delle Alpi nordoccidentali interne: *Memorie della Società Geologica Italiana*, v. 11, pp.  
612 433–460.
- 613 Decandia, F.A., and Elter, P., 1972, La “zona” ofiolitifera del Bracco nel settore compreso fra Levanto  
614 e la Val Graveglia (Appennino ligure): *Memorie della Società Geologica Italiana*, v. 11, pp. 503–  
615 530.
- 616 De Wever P. and Baumgartner P.O., 1995, Radiolarians from the base of the supra-ophiolitic Schistes  
617 Lustrés formation in the Alps (Saint-Véran, France and Traversiera Massif, Italy), in Baumgartner  
618 P.O. et al., eds., *Middle Jurassic to Lower Cretaceous radiolaria of Tethys: occurrences,*  
619 *systematics, biochronology: Memoire Géologique, Lausanne*, v.23, pp. 725–730.
- 620 Dick, H.J.B., Tivey, M.A., and Tucholke, B.E., 2008, Plutonic foundation of a slow-spreading ridge  
621 segment: Oceanic core complex at Kane Megamullion, 23\_300N, 45\_200W: *Geochemistry,*  
622 *Geophysics, Geosystems*, v. 9, Q05014, doi:10.1029/2007GC001645.
- 623 Dilek, Y., 2006, Collision tectonics of the Eastern Mediterranean region: Causes and  
624 consequences: *Geological Society of America Special Paper*, v. 409, pp. 1-13.
- 625 Dilek, Y. and Delaloye, M., 1992, Structure of the Kizildag ophiolite, a slow-spread Cretaceous ridge  
626 segment north of the Arabian promontory: *Geology*, v. 20, pp. 19-22.
- 627 Dilek, Y. and Eddy, C.A., 1992, The Troodos (Cyprus) and Kizildag (S. Turkey) ophiolites as structural  
628 models for slow-spreading ridge segments: *Journal of Geology*, v. 100, pp. 305-322.
- 629 Dilek, Y., Coulton, A., and Hurst, S., 1997, Serpentinization and hydrothermal veining in  
630 peridotites at Site 920 in the MARK area (Leg 153): In, Cannat, J. Karson, J. Miller,  
631 and D. Elthon, eds., *Proceedings of the Ocean Drilling Program, Scientific Results*, v. 153:  
632 *College Station, Texas (Ocean Drilling Program)*, pp. 35-59.
- 633 Dilek, Y., Moores, E.M., and Furnes, H., 1998, Structure of modern oceanic crust and ophiolites and  
634 implications for faulting and magmatism at oceanic spreading centers: In, Buck, R., Karson, J.,  
635 Delaney, P., and Lagabriele, Y., eds., *AGU Monograph on Faulting and Magmatism at Mid-Ocean*  
636 *Ridges*, v. 106, pp. 219-266.
- 637 Dilek, Y. and Thy, P., 1998, Structure, petrology, and seafloor spreading tectonics of the Kizildag  
638 ophiolite (Turkey). In, Mills, R., and Harrison, K., eds., *Modern Ocean Floor Processes and the*  
639 *Geological Record: Geological Society of London Special Publication*, v. 148, pp. 43-69.
- 640 Dilek, Y. and Newcomb. S., 2003, Ophiolite Concept and the Evolution of Geological Thought:  
641 *Geological Society of America Special Paper*, v. 373, 504 pp. ISBN 0-8137-23736.
- 642 Dilek, Y. and Furnes, H., 2011, Ophiolite genesis and global tectonics: geochemical and tectonic  
643 fingerprinting of ancient oceanic lithosphere: *The Geological Society of America Bulletin*, v. 123,  
644 pp. 387-411, DOI: 10.1130/B30446.1.
- 645 Dilek, Y., and Furnes, H., 2014, Ophiolites and their origins: *Elements*, v. 10, p. 93–100,  
646 doi:10.2113/gselements.10.2.93.
- 647 Elter G., 1971, Schistes lustrés et ophiolites de la zone piemontaise entre Orco et Doire Baltée (Alpes  
648 Graies). Hypotèses sur l'origine des ophiolites: *Géologie Alpine*, v. 47, pp. 147-169.
- 649 Escartin, J., and Canales, J.P., 2011, Detachments in oceanic lithosphere: Deformation, magmatism,  
650 fluid flow and ecosystems: *Eos, Transactions, American Geophysical Union*, v. 92, pp.31,  
651 <http://dx.doi.org/10.1029/2011EO040003>.



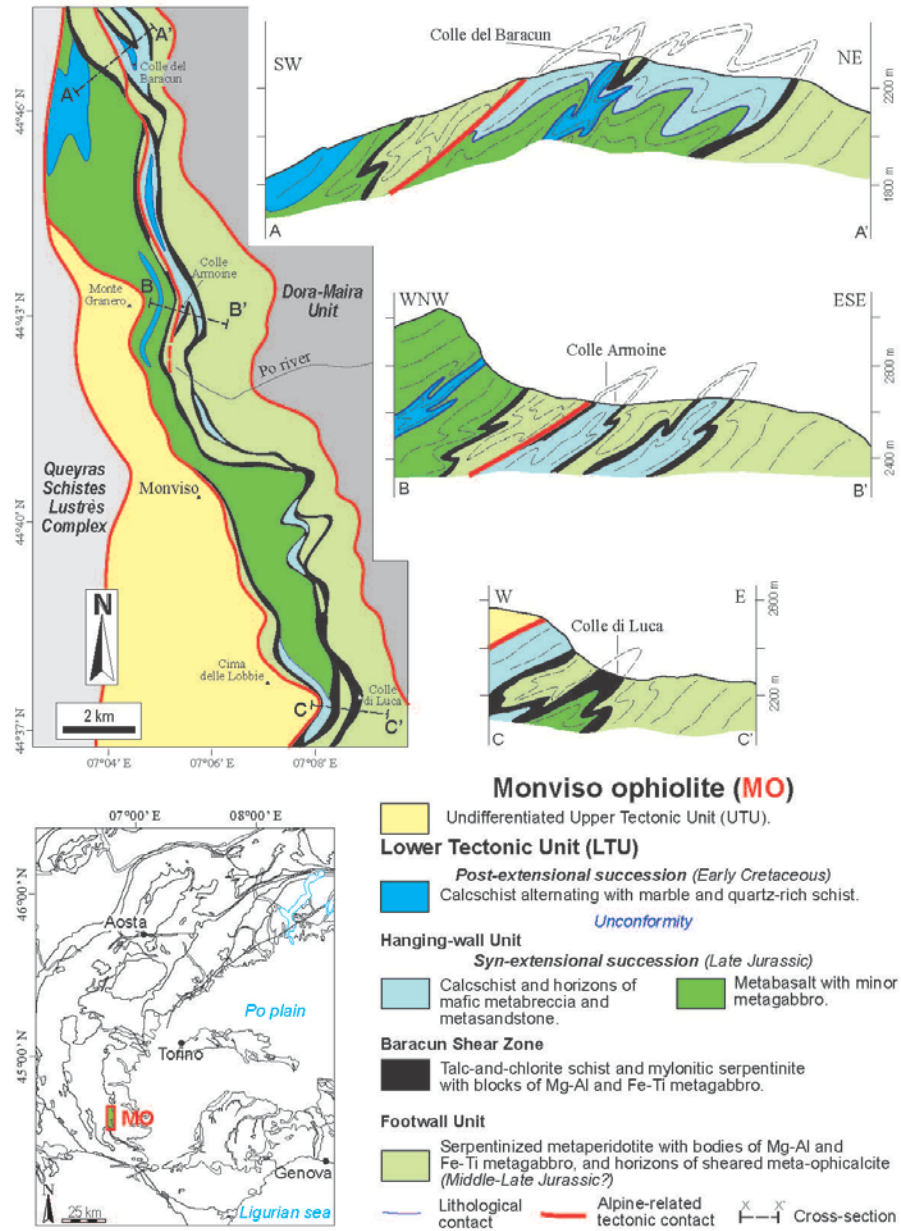
- 652 Escartin, J., Smith, D.K., Cann, J., Schouten, H., Langmuir, C.H., and Escrig, S., 2008, Central role of  
653 detachment faults in accretion of slowspread oceanic lithosphere: *Nature*, v. 455, pp. 790–794,  
654 doi:10.1038/nature07333.
- 655 Fantoni, R., Bersezio, R., and Forcella, F., 2004, Alpine structure and deformation chronology at the  
656 Southern Alps-Po Plain border in Lombardy: *Bollettino della Società Geologica Italiana*, v. 123, pp.  
657 463-476.
- 658 Fantoni, R., Decarlis, A., and Fantoni, E., 2003, L'estensione mesozoica al margine occidentale delle  
659 Alpi meridionali (Piemonte settentrionale, Italia): *Atti Ticinensi di Scienze della Terra*, v. 44, pp. 97-  
660 110.
- 661 Festa, A., 2011, Tectonic, sedimentary, and diapiric formation of the Messinian mélange: Tertiary  
662 Piedmont Basin (northwestern Italy), in Wakabayashi, J., and Dilek, Y., eds., *Mélanges: Processes  
663 of Formation and Societal Significance: Geological Society of America Special Paper 480*, pp.  
664 215–232, doi:10.1130/2011.2480(10).
- 665 Festa A., Balestro, G., Dilek Y, and Tartarotti, P., 2015a, A Jurassic oceanic core complex in the high-  
666 pressure Monviso ophiolite (western Alps, NW Italy): *Lithosphere*, v.7, 646-652, Doi:  
667 10.1130/L458.1.
- 668 Festa A., Dilek., Y., Codegone G., Cavagna, S., and Pini, G.A., 2013, Structural Anatomy of the  
669 Ligurian Accretionary Wedge (Monferrato, NW-Italy), and Evolution of Superposed Mélanges:  
670 *Geological Society of America Bulletin*, v. 125 (9/10), pp. 1580-1598. Doi: 10.1130/B30847.1
- 671 Festa, A., Dilek, Y., Pini, G.A., Codegone, G., and Ogata, K., 2012, Mechanisms and processes of  
672 stratal disruption and mixing in the development of mélanges and broken formations: redefining  
673 and classifying mélanges: *Tectonophysics*, v. 568-569, pp. 7-24. DOI:  
674 10.1016/j.tecto.2012.05.021.
- 675 Festa A., Fioraso G, Bissacca E., and Petrizzo M.R., 2015b, Geology of the Villalvernia-Varzi Line  
676 between Scrivia and Curone valleys (NW Italy), in Zucali M., and Spalla, I., eds., *Structural  
677 Mapping in the Mediterranean: bridging laboratory to lithosphere: Journal of Maps*, v. 11 (1), pp.  
678 39-55. Doi: 10.1080/17445647.2014.959569.
- 679 Festa, A., Ogata, K., Pini, G.A., Dilek, Y., and Codegone, G., 2015c, Late Oligocene – early Miocene  
680 olistostromes (sedimentary mélanges) as tectono-stratigraphic constraints to the geodynamic  
681 evolution of the exhumed Ligurian accretionary complex (Northern Apennines, NW Italy):  
682 *International Geology Review*, v. 57, no. 5-8, pp. 540-562. Doi: 10.1080/00206814.2014.931260.
- 683 Funicello, R., Parotto, M., Praturlon, A., and Bigi, G., 1981, Carta tettonica d'Italia – schema  
684 preliminare: CNR-Consiglio Nazionale delle Ricerche. Ed. Grafica editoriale cartografica, Roma. 1  
685 sheet. 1:1.500.000 scale.
- 686 Frey, M., Desmons, J. and Neubauer, F., eds, 1999, The new metamorphic map of the Alps:  
687 *Schweizerische Mineralogische und Petrographische Mitteilungen*, v. 79, pp. 1-230.
- 688 Ghibardo, G., Massari, F., and Chiambretti, I., 2014, Oligo-Miocene tectono-sedimentary evolution of  
689 the Langhe Sub-basin: from continental basinal setting (Tertiary Piedmont Basin – Northwestern  
690 Italy): *Journal of Mediterranean Earth Sciences*, v. 6, pp. 53-144.
- 691 Ghielmi, M., Minervini, M., Nini, C., Rogledi, S., and Rossi, M., 2013, Late Miocene – Middle  
692 Pleistocene sequences in the Po Plain – Northern Adriatic Sea (Italy): The stratigraphic record of  
693 modification phases affecting a complex foreland basin: *Marine and Petroleum Geology*, v. 42, pp.  
694 50-81.
- 695 Groppo, C., and Castelli, D., 2010, Prograde P–T evolution of a lawsonite eclogite from the Monviso  
696 Meta-ophiolite (Western Alps): Dehydration and redox reactions during subduction of oceanic  
697 FeTi-oxide gabbro: *Journal of Petrology*, v. 51, pp. 2489–2514. doi:10.1093/petrology/egq065.
- 698 Guillot, S., Hattori, K., Agard, P., Schwartz, S., and Vidal, O., 2009, Exhumation processes in oceanic  
699 and continental subduction contexts: A review, in Lallemand, S., and Funicello, F., eds.,  
700 *Subduction zone geodynamics: Berlin Heidelberg, Springer-Verlag*, pp. 275.
- 701 Kaczmarek, M.-A., Müntener, O., Rubatto, D., 2008, Trace element chemistry and U–Pb dating of  
702 zircons oceanic gabbros and their relationship with whole rock composition (Lanzo, Italian Alps):  
703 *Contributions to Mineralogy and Petrology*, v. 155, pp. 295–312.

- 704 Karson J.A., Fruh-Green, G.L., Kelley, D.S., Williams, E.A., Yoerger, D.R. and Jakuba, M., 2006,  
705 Detachment shear zone of the Atlantis Massif core complex, Mid-Atlantic Ridge, 30°N:  
706 Geochemistry, Geophysics, Geosystems, v.7(6), Q06016, doi: 10.1029/2005GC001109.
- 707 Lagabrielle, Y., 1994, Ophiolites of the southwestern Alps and the structure of the Tethyan oceanic  
708 lithosphere: *Ophioliti*, v. 19, 413–434.
- 709 Lagabrielle, Y., 2009, Mantle exhumation and lithosphere spreading: An historical perspective from  
710 investigations in the oceans and in the Alps-Apennines ophiolites: *Italian Journal of Geosciences*,  
711 v. 128 (2), pp. 279-293.
- 712 Lardeaux, J., Schwartz, S., Tricart, P., Paul, A., Guillot, S., Béthoux, N., and Masson, F., 2006, A  
713 crustal-scale cross-section of the south-western Alps combining geophysical and geological  
714 imagery: *Terra Nova*, v. 18, no. 6, pp. 412–422. doi:10.1111/j.1365-3121.2006.00706.x
- 715 Lafay, R., Deschamps, F., Scghwartz, S., Guillot, S., Godard, M., Debret, B., and Nicollet, C., 2013,  
716 High-pressure serpentinites, a trap-and-release system controlled by metamorphic conditions:  
717 Example from the Piedmont zone of the western Alps: *Chemical Geology*, v. 343, pp. 38-54.
- 718 Laubscher, H.P., 1991, The arc of Western Alps today: *Eclogae Geologicae Helvetiae*, v. 84, pp. 631–  
719 659.
- 720 Lemoine, M., 1971, Données nouvelles sur la série du Gondran près Briançon (Alpes Cottiennes).  
721 Réflexions sur les problèmes stratigraphique et paléogéographique de la zone piémontaise:  
722 *Géologie Alpine*, v. 47, pp. 181-201.
- 723 Lemoine, M., and Tricart, P., 1986, Les schistes lustrés piémontais des Alpes occidentales: approche  
724 stratigraphique, structurale et sédimentologie: *Eclogae Geologicae Helvetiae*, v. 79, pp. 271–294.
- 725 Liati, A., Froitzheim, N., and Fanning, C.M., 2005, Jurassic ophiolites within the Valais domain of the  
726 Western and Central Alps: geochronological evidence for re-rifting of oceanic crust: *Contributions*  
727 *to Mineralogy and Petrology*, v. 149 (4), pp. 446–461.
- 728 Lombardo, B., Nervo, R., Compagnoni, R., Messiga, B., Kienast, J., Mevel, C., Fiora, L., Piccardo, G.,  
729 and Lanza, R., 1978, Osservazioni preliminari sulle ofioliti metamorfiche del Monviso (Alpi  
730 Occidentali): *Rendiconti Società Italiana Di Mineralogia E Petrologia*, v. 34, pp. 253–305.
- 731 Lombardo, B., Rubatto, D., and Castelli, D., 2002, Ion microprobe U–Pb dating of zircon from a  
732 Monviso metaplagiogranite: Implications for the evolution of the Piedmont-Liguria Tethys in the  
733 Western Alps: *Ophioliti*, v. 27, pp. 109–117.
- 734 MacLeod, C.J., Escartin, J., Banerji, D., Banks, G.J., Gleeson, M., Irving, D.H.B., Lilly, R.M., McCaig,  
735 A.M., Niu, Y., Allerton, S., and Smith, D.K., 2002, Direct geological evidence for oceanic  
736 detachment faulting: The Mid-Atlantic Ridge, 15\_450N: *Geology*, v 30, pp. 879–882.
- 737 Maffione, M., Thieulot, C., van Hinsbergen, D.J.J, Morris, A., Plumper, O., and Spakman, W., 2015,  
738 Dynamics of intra-oceanic subduction initiation. 1: Oceanic detachment fault inversion and the  
739 formation of forearc ophiolites: *Geochemistry, Geophysics, Geosystems*, v. 16 (6), pp. 1753-1770.  
740 doi:10.1002/2015GC005746.
- 741 Manatschal, M., and Müntener, O., 2009, A type sequence across an ancient magma-poor ocean–  
742 continent transition: the example of the western Alpine Tethys ophiolites: *Tectonophysics*, v. 473,  
743 pp. 4–19.
- 744 Manatschal, G., Engstrom, A., Desmurs, L., Schaltegger, U., Cosca, M., Müntener, O., and Bernoulli,  
745 D., 2006. What is the tectono-metamorphic evolution of continental break-up: the example of the  
746 Tasna Ocean–Continent Transition: *Journal of Structural Geology*, v. 28 (10), pp. 1849–1869.
- 747 Manatschal, G., Sauter, D., Karpoff, A.M., Masini, E., Mohn, G., and Lagabrielle, Y., 2011,  
748 TheChenaillet Ophiolite in the French/Italian Alps: an ancient analogue for an Oceanic Core  
749 Complex?: *Lithos*, v. 124, pp. 169–184. <http://dx.doi.org/10.1016/j.lithos.2010.10.017>.
- 750 Manzotti, P., Ballèvre, M., Zucali, M., Robyr, M. and Engi, M., 2014, The tectonometamorphic  
751 evolution of the Sesia-Dent Blanche nappes (internal Western Alps): review and synthesis: *Swiss*  
752 *Journal of Geosciences*, v.107, pp. 309-336.
- 753

- 754 Marroni, M., Meneghini, F., and Pandolfi, L., 2010, Anatomy of the Ligure-Piemontese subduction  
755 system: Evidence from Late Cretaceous–middle Eocene convergent margin deposits in the  
756 Northern Apennines, Italy: *International Geology Review*, v. 52, pp. 1160–1192.
- 757 Michard, A., Goffe, B., Chopin, C., and Henry, C., 1996, Did the Western Alps develop through an  
758 Oman-type stage? The geotectonic setting of high-pressure metamorphism in two contrasting  
759 Tethyan transects: *Eclogae Geologicae Helvetiae*, v. 89, pp. 43– 80.
- 760 Miranda, E.A. and Dilek, Y., 2010, Oceanic core complex development in modern and ancient oceanic  
761 lithosphere: Gabbro-localized versus peridotite-localized detachment models: *Journal of Geology*,  
762 v. 118, pp. 95-109, DOI: 10.1086/648460.
- 763 Péron-Pinvidic, G., and Manatschal, G., 2009, The final rifting evolution at deep magma-poor passive  
764 margins from Iberia-Newfoundland: a new point of view: *International Journal of Earth Sciences*, v.  
765 98, pp. 1581-1597.
- 766 Perrone, G., Cadoppi, P., and Tallone, S., 2015, Geometry and impact of transpressional faulting in  
767 polyphasic metamorphic orogenic belts: the Viù Deformation Zone (inner Western Alps):  
768 *International Geology Review*, v. 50 (11), pp. 1022-1039. doi: 10.1080/00206814.2015.1033655.
- 769 Piccardo, G., 2009, Evolution of the lithospheric mantle in an extensional setting: Insights from  
770 ophiolitic peridotites: *Lithosphere*, v.1, pp. 81-87.
- 771 Platt, J.P., Behrmann, J.H., Cunningham, P.C., Dewey, J.F., Helman, M., Parish, M., Shepley, M.G.,  
772 Wallis, S., and Western, P.J., 1989, Kinematics of the Alpine arc and the motion history of Adria:  
773 *Nature*, v. 337, pp. 158–161. doi:10.1038/337158a0.
- 774 Ricou, L.E., and Siddans, W.B., 1986, Collision tectonics in the western Alps: Geological Society,  
775 London, Special Publications, v. 19, pp. 229–244. doi:10.1144/GSL.SP.1986.019.01.13.
- 776 Rubatto, D., and Hermann, J., 2003, Zircon formation during fluid circulation in eclogites (Monviso,  
777 Western Alps): implications for Zr and Hf budget in subduction zones: *Geochimica et*  
778 *Cosmochimica Acta*, v. 67 (12), pp. 2173–2187.
- 779 Rubatto, D., Gebauer, D., Fanning, M., 1998. Jurassic formation and Eocene subduction of the  
780 Zermatt–Saas-Fee ophiolites: implications for the geodynamic evolution of the Central and  
781 Western Alps: *Contributions to Mineralogy and Petrology*, v. 132, pp. 269–287.
- 782 Schmid, S.M., and Kissling, E., 2000, The arc of the western Alps in the light of geophysical data on  
783 deep crustal structure: *Tectonics*, v. 19, pp. 62–85. doi:10.1029/1999TC900057.
- 784 Stampfli, G.M. and Marthaler, M., 1990, Divergent and convergent margins in the North-Western Alps  
785 confrontation to actualistic models: *Geodynamica Acta*, v. 4., pp. 159-184.
- 786 Stucki, A., Rubatto, D., and Trommsdorff, V., 2003, Mesozoic ophiolite relics in the Southern Steep  
787 Belt of the Central Alps. *Schweizerische Mineralogische und Petrographische Mitteilungen*, v. 83,  
788 pp. 285–299.
- 789 Tricart, P., and Lemoine, M., 1991, The Queyras ophiolite west of Monte Viso (Western Alps):  
790 indicator of a peculiar ocean floor in the Mesozoic Tethys: *Journal of Geodynamics*, v. 13, pp.163–  
791 181.
- 792 Tricart, P., and Schwartz, S., 2006, A north-south section across the Queyras Schistes lustrés  
793 (Piedmont zone, western Alps): Syn-collision refolding of a subduction wedge: *Eclogae*  
794 *Geologicae Helvetiae*, v. 99, pp. 429–442.
- 795 Tucholke, B., Lin, J. and Kleinrock, M.C., 1998, Megamullions and mullion structure defining oceanic  
796 metamorphic core complexes on the Mid-Atlantic Ridge: *Journal of Geophysical Research*, v. 103,  
797 pp. 9857-9866.
- 798

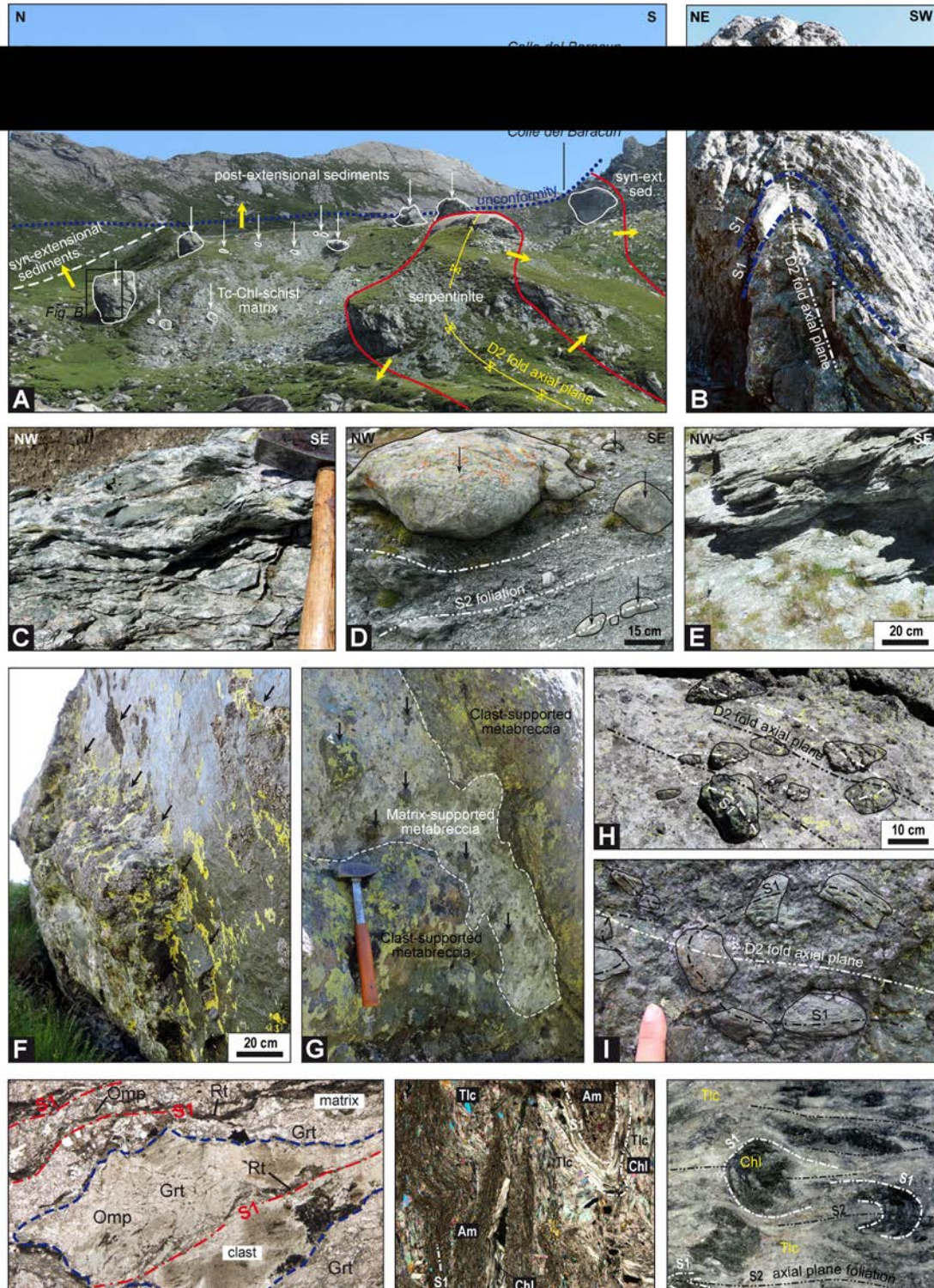






809  
810  
811  
812  
813  
814  
815  
816  
817

**Figure 2** – Geological map and structural cross-sections (A-A' through C-C") of the Lower Tectonic Unit (LTU) of the Monviso ophiolite (MO) (modified from Balestro et al., 2011, 2013, 2014, 2015), depicting the geometry of the Baracun Shear Zone (BSZ), its hanging wall and footwall units and the post-extensional metasedimentary sequence. The index map shows the location of the Monviso geological map and the geography of the Western Alps.



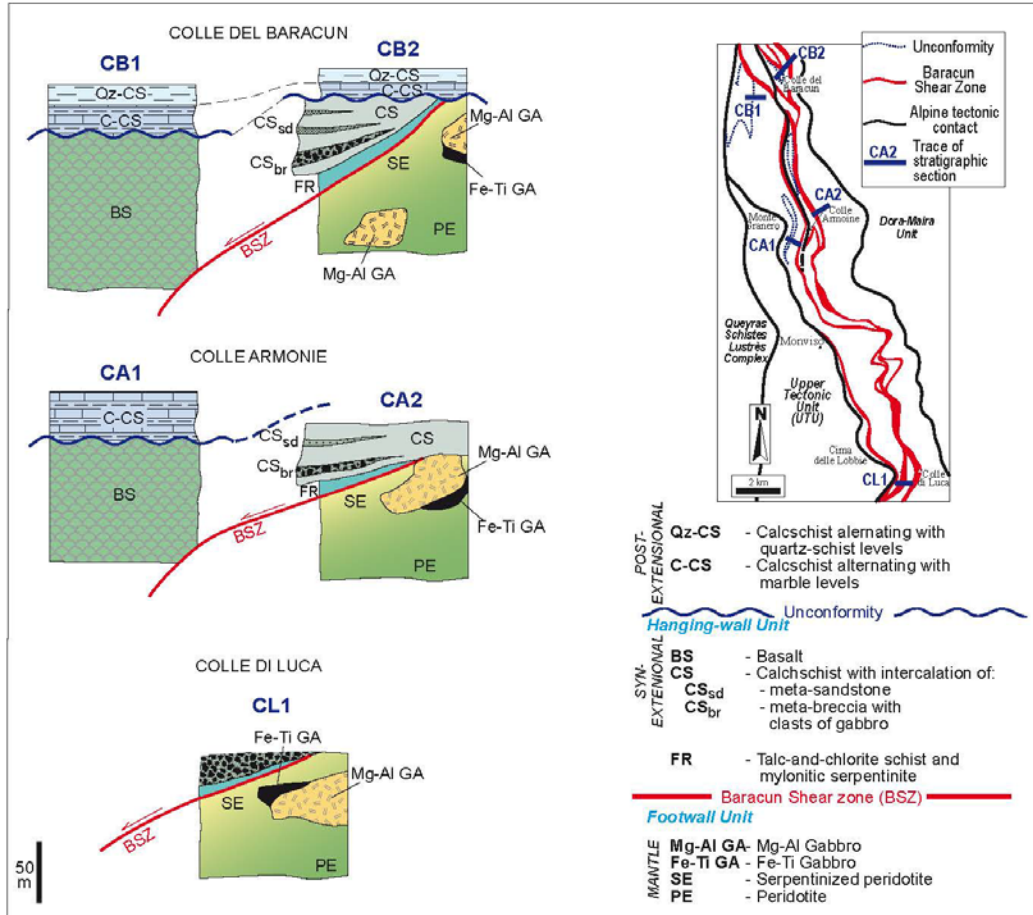
818  
819

820 **Figure 3** – Images of the Baracun Shear Zone (BSZ) and structures at different scales: (A) Panoramic  
821 view of the BSZ at the Colle del Baracun, showing its block-in-matrix fabric. White arrows point to the  
822 blocks of Fe-Ti and Mg-Al metagabbros, and to some rare blocks of metarenite embedded in a matrix  
823 of talc-chlorite schist. Yellow arrows indicate the younging direction of the primary sedimentary  
824 sequence, now folded by Alpine deformation. Post-extensional sedimentary rocks rest unconformably  
825 (dotted blue line) on both the syn-extensional sequence and the talc-chlorite schist of the BSZ; (B)



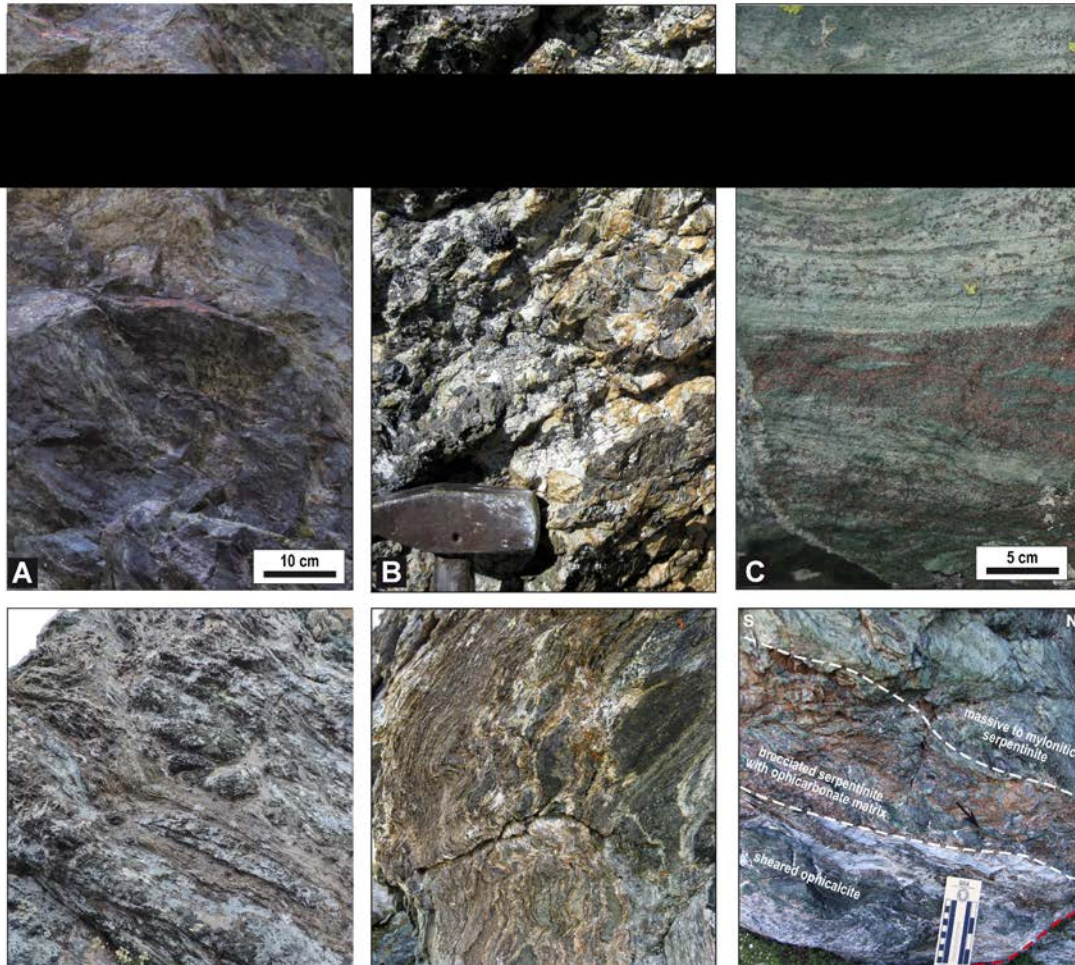
826 Close-up photo of one of the larger metagabbro blocks embedded within the BSZ matrix (location in  
827 Fig. 3A). The shape of the block corresponds to the fold hinge of a D2 fold, which deformed the  
828 previously formed foliation S1. Note the mafic metabreccia enveloping the block (see also Figs. 3F,  
829 3G, 3I, 3L). Hammer for scale; (C) Close-up of the structural fabric of the talc-chlorite schist matrix at  
830 Colle del Baracun (hammer as scale); (D) Close-up of the block-in-matrix fabric of the BSZ at Colle  
831 di Luca. Rounded to elongated blocks of gabbro (black arrows) are embedded within a mylonitic  
832 serpentinite matrix affected by D2 foliation (dashed white lines); (E) Talc-chlorite schist matrix of the  
833 BSZ at Colle di Luca; (F) Close-up of a Fe-Ti metagabbro block within the BSZ, enveloped by a dm-  
834 thick horizon of a clast-supported mafic metabreccia outcrop (black arrows), with clasts of the same  
835 composition as in the main block (Colle del Baracun); (G) Close-up of the contact between the clast-  
836 supported mafic metabreccia enveloping the metagabbro blocks and the talc-chlorite schist matrix,  
837 embedding rounded blocks of metagabbro, centimeters to decimeters in size (Colle di Luca). Hammer  
838 as scale; (H and I) Close-up of the mafic metabreccia enveloping blocks of gabbro. Note that  
839 irregularly shaped clasts, centimeters to decimeters in size, preserve an earlier formed foliation, S1,  
840 folded by D2 deformation (Colle di Luca and Colle del Baracun, respectively); (L) Photomicrograph  
841 showing the clast/matrix relationship within the mafic metabreccia of Figure 3I (modified after Balestro  
842 et al., 2015). The matrix and the irregularly shaped clast (dashed blue line) are affected by S1 foliation  
843 (dashed red line), which is defined by an eclogite-facies mineral assemblage (i.e. garnet, omphacite,  
844 and rutile); (M) Photomicrograph of talc-chlorite schist in the BSZ at Colle del Baracun, showing  
845 amphibole- (Amp), chlorite- (Chl) and talc-rich (Tlc) domains folded by tight to isoclinal D2 folds. Note  
846 the folded S1 foliation (dashed white lines); (N) Close-up of a polished hand sample of the talc-chlorite  
847 schist matrix (Colle del Baracun), showing rootless D2 fold hinges in chlorite-rich (Chl) domains,  
848 overprinting the early S1 foliation (dashed white lines). S2 axial planar foliation (dashed black lines)  
849 occurs in talc-rich (Tlc) domains.  
850





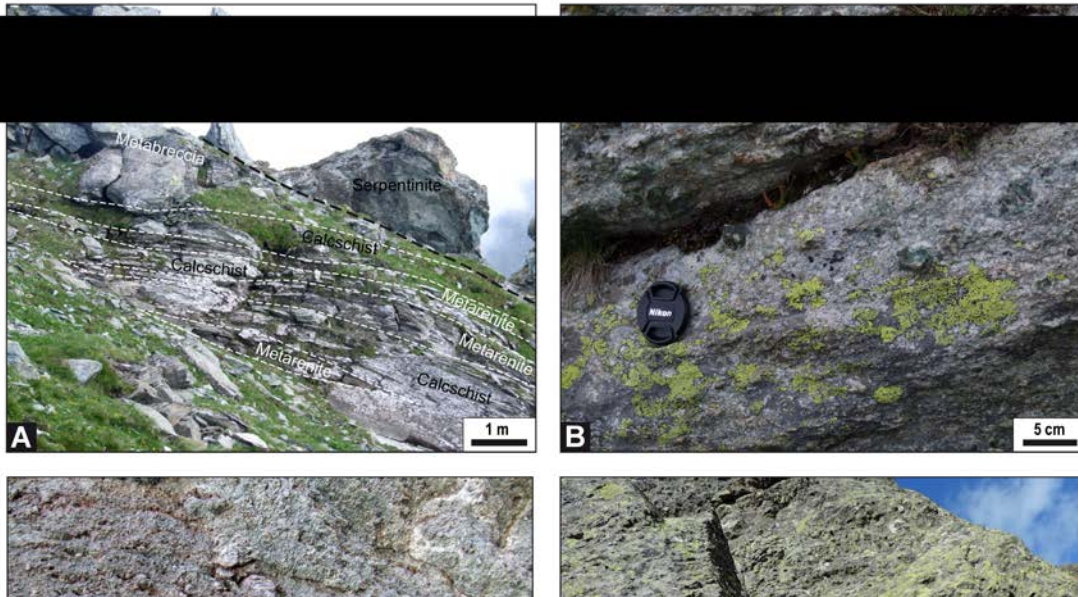
851  
852  
853  
854  
855  
856  
857

**Figure 4** – Simplified stratigraphic columnar sections, showing the tectono-stratigraphic relationships between the hanging wall – footwall units and the BSZ (traces are shown in the simplified geological map).



858  
859  
860  
861  
862  
863  
864  
865  
866  
867  
868  
869  
870  
871  
872  
873  
874  
875  
876  
877  
878  
879  
880  
881

**Figure 5** – Field images of various lithologies and structures in the BSZ footwall unit: (A) Medium-grained, massive serpentinite with a lherzolitic protolith (East of Colle del Baracun); (B) Close-up of a pegmatitic, coarse-grained Mg-Al metagabbro (South of Colle Armoine). Hammer head as scale; (C) Close-up of a foliated, Mg-Al metagabbro with reddish Fe-Ti layers (W of Colle di Luca); (D) Sheared metaophicalcinate with light-brown carbonate layers, deformed by D2 folds (East of Colle Armoine); (E) Sheared meta-ophicalcinate marking the contact between the footwall sequence and the BSZ. Ophicalcinate rocks consist of serpentinite (dark green) meshed with white, cm to mm-thick hydrothermal calcite veins (South of Colle di Luca); (F) Close-up view of the overturned tectonic contact between the massive serpentinite in the footwall unit and the talc-chlorite schist within the BSZ at the Colle del Baracun. Note the progressive transition from the massive serpentinite to the pervasively sheared talc-chlorite schist.

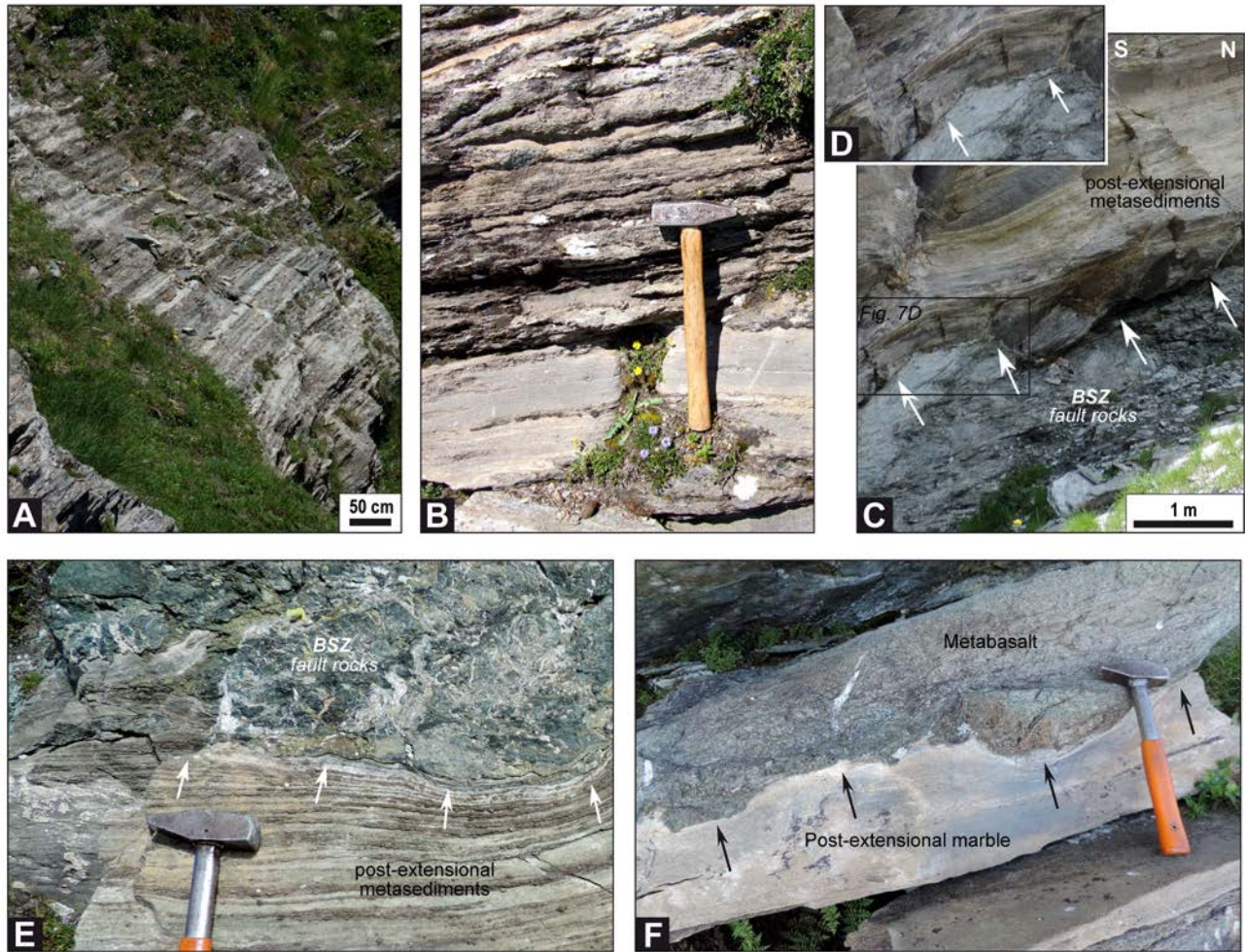


882  
883  
884  
885  
886  
887  
888  
889  
890  
891  
892  
893  
894  
895  
896  
897  
898  
899  
900  
901  
902  
903  
904  
905  
906  
907  
908  
909  
910  
911  
912

**Figure 6** – Field images of various lithologies, contact relationships and structures in the BSZ hanging wall unit: (A) Panoramic view of the overturned mantle rocks and the cover sequence to the South of Colle del Baracun. Metasedimentary rocks consists of intercalations of mafic metabreccia and metasandstone horizons (dashed white lines), decimeters to several meters thick, that are interbedded with medium to coarse-grained calcschist; (B) Close-up photo of the detrital texture of a matrix-supported mafic metabreccia layer characterized by rounded clasts, centimeters in size, embedded in the coarse-grained mafic matrix (NE of Colle del Baracun); (C) Close-up image of a fining-upward, matrix-supported, mafic metabreccia passing upward into a metasandstone rock (overturned sequence). Note the rounded shape of clasts (Colle del Baracun); (D) Metabasaltic rock with a relict brecciated texture (hammer for scale) (West of Colle Armoine).



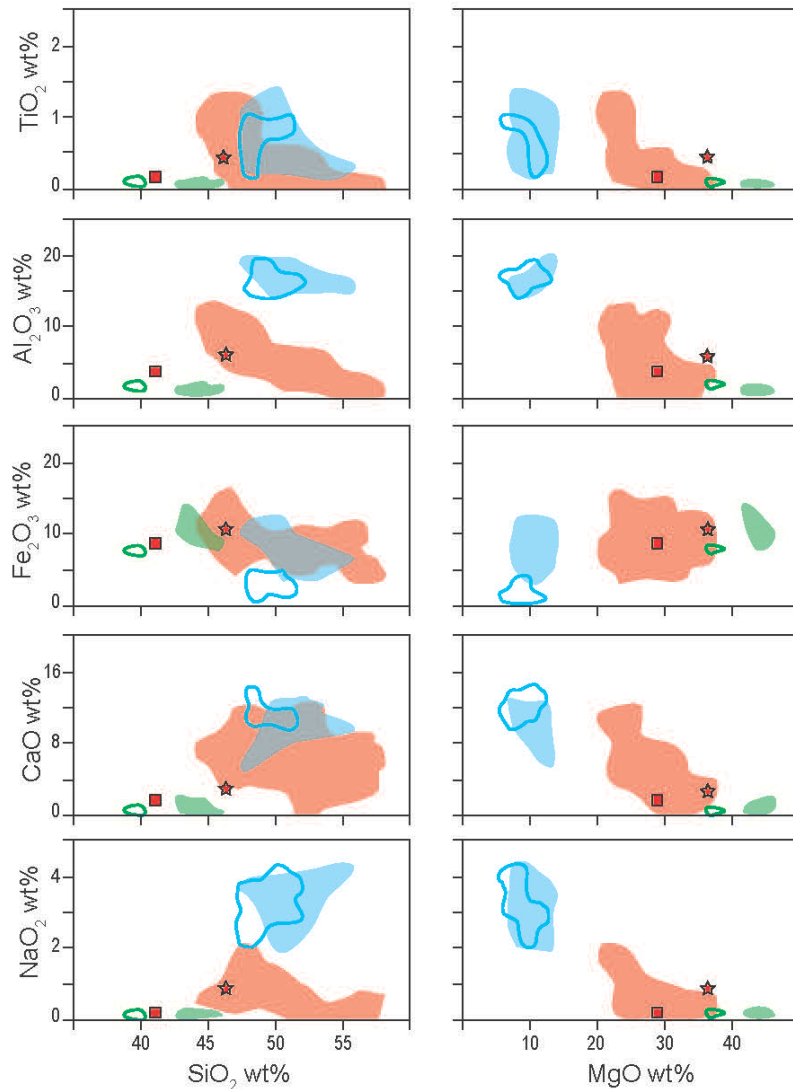
913



914  
 915  
 916  
 917  
 918  
 919  
 920  
 921  
 922  
 923  
 924  
 925  
 926  
 927  
 928  
 929  
 930  
 931  
 932  
 933  
 934

**Figure 7** – Field images of various lithologies, contact relationships and structures in the post-extensional sedimentary sequence: (A) Panoramic view of the post-extensional sequence in the Colle del Baracun section, consisting of calcschist alternating with dm-thick marble layers; (B) Close-up of the outcrop in A, showing a dm-thick marble layer interbedded with calcschist (hammer for scale); (C, D, E) Different views of the post-extensional sequence, unconformably resting on the BSZ at Colle del Baracun. Note that the sequence is overturned in E; (F) Close-up photo of the overturned primary contact (black arrows) between a metabasalt and a white marble in the postextensional sequence (hammer for scale) (West of Colle Armoine).

935



936

937

938

939

940

941

942

943

944

945

946

947

948

949

950

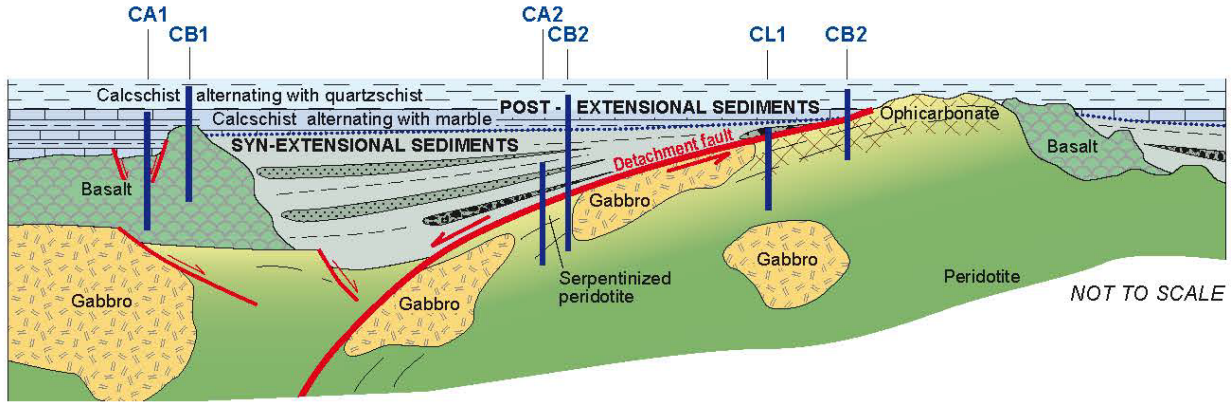
951

952

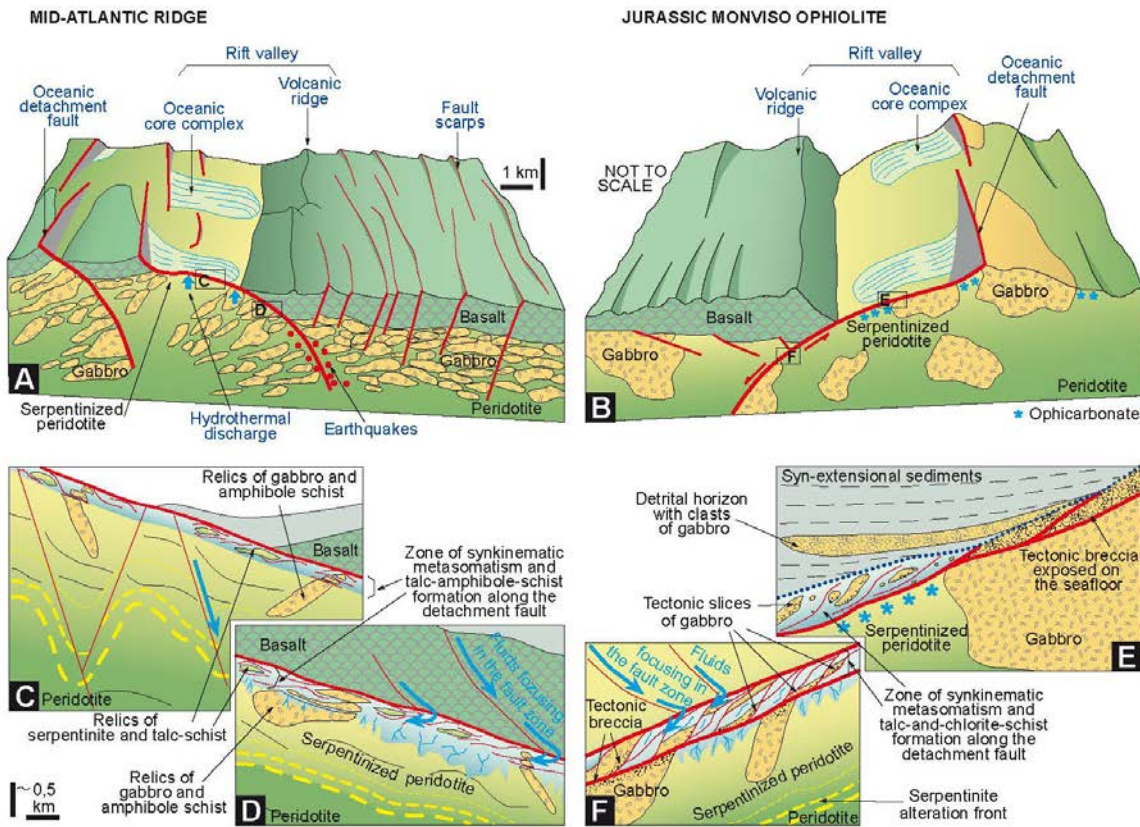
953

**Figure 8** – Harker-type (SiO<sub>2</sub> and MgO) and major-element variation diagrams of the talc-chlorite schist (red square) of the BSZ matrix. Green, red and light blue shaded areas show the compositional ranges of serpentinite, talc-chlorite schist and gabbro from the Atlantis Massif, respectively (modified from Boschi et al., 2006). Green and light-blue lines show the compositional ranges of serpentinitized metaperidotites and metagabbros from the Monviso ophiolite, respectively (modified from Lombardo et al., 1978, Lafay et al., 2013).

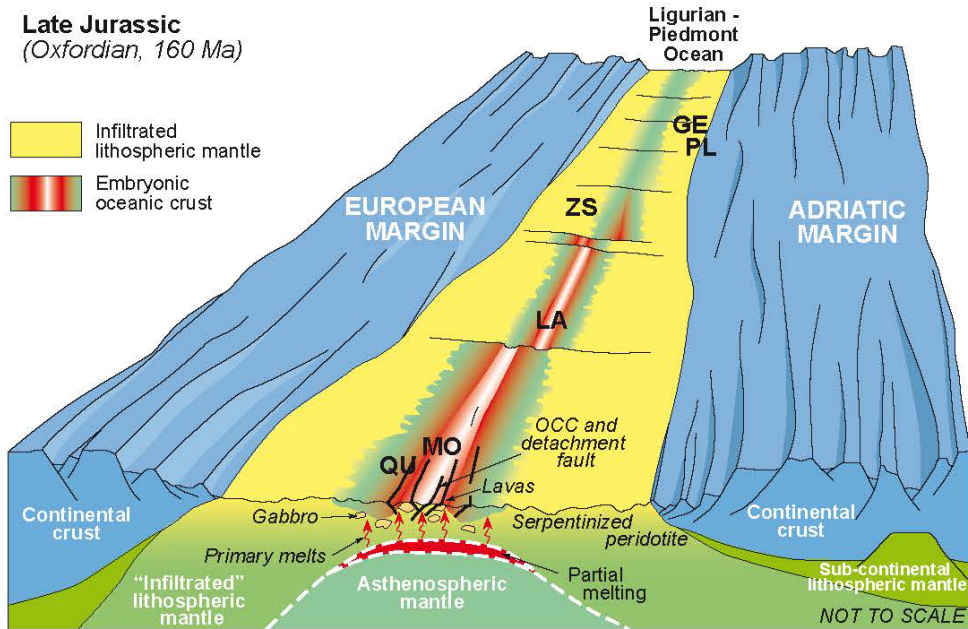




954  
 955 **Figure 9** – Interpretive reconstruction of the Monviso ophiolite oceanic core complex, constrained by  
 956 the analysis of the metasedimentary sequence and by the observed structural relationships between  
 957 the hanging wall and footwall units of the extensional detachment fault (Baracun Shear Zone). Thick  
 958 vertical blue lines (and related acronyms) indicate the approximate locations of the stratigraphic  
 959 columnar sections shown in Figure 4.  
 960



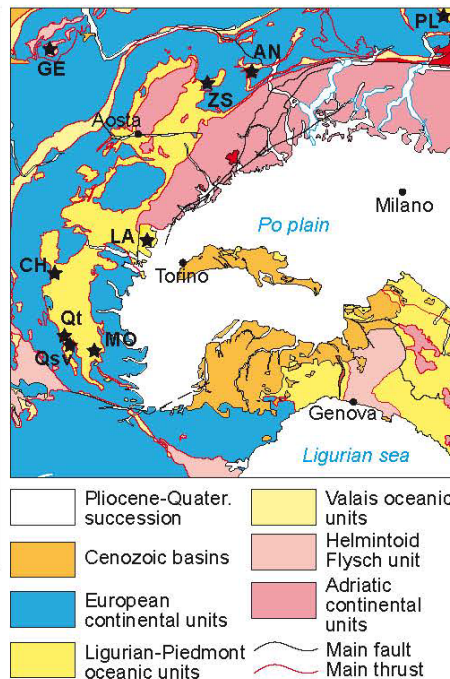
961  
 962  
 963 **Figure 10** – Comparison between (A) an in-situ, intra-oceanic core complex along the Mid-Atlantic  
 964 Ridge (modified from Escartin and Canales, 2011), and (B) the inferred Monviso oceanic core complex  
 965 developed within the Jurassic Ligurian-Piedmont Ocean. (C-F) Close up cross sections of a  
 966 detachment fault system (location in Figs 10A and 10B) and associated metasomatic and tectonic-  
 967 processes in modern (C-D; modified from Boschi et al., 2006) and ancient oceanic (E-F)  
 968 settings, respectively.



Period	JURASSIC					
Epoch	Middle			Late		
Age	Bajocian	Bathonian	Callovian	Oxfordian	Kimmerid.	Tithonian
Age (Ma)	170	165	160	155	150	
Gets (GE)		+				
Zermatt-Saas (ZS)		—	—	—	—	—
Queyras (QU)		—	—	—		
Monviso (MO)		—	—		+	
Lanzo (LA)		—	—	—	—	
Platta (PL)			+			
Chenaillet (CH)				—	—	+
Antrona (AN)				—	—	

(meta)gabbro	plagiogranite
albitite	diorite
Mn-rich metasediments and metaradiolarite	



970  
 971  
 972  
 973  
 974  
 975  
 976  
 977  
 978  
 979  
 980  
 981

**Figure 11** – Interpretive block diagram depicting the inferred paleogeography of the Monviso ophiolite ridge segment (MO) in the Ligurian-Piedmont Ocean in the Late Jurassic (Oxfordian, 160 Ma). Frontal cross-section modified from Dilek and Furnes (2011), Piccardo et al. (2009), Peron-Pinvidic and Manatschal (2009). Table in the lower left-side displays the known age ranges of mafic rocks, Mn-rich metasedimentary rocks, and meta-radiolarite from the Ligurian–Piedmont oceanic lithosphere (data sources: Borsi et al., 1996; Caby et al., 1987; Costa and Caby, 2001; De Wever and Beumagarter, 1995; Kaczmarek et al., 2008; Liati et al., 2005; Lombardo et al., 2002; Manatschal et al., 2006; Rubatto and Hermann, 2003; Rubatto et al., 1998; Stuki et al., 2003). Geological map of the Alps and the Northern Apennines shows the present-day location of the tectonostratigraphic units used in the entire figure.